OPTICAL METROLOGY OF FREEFORM OPTICS UTILIZING INTERFEROMETRIC STITCHING

by

Clark Hovis

A thesis submitted to the faculty of
The University of North Carolina at Charlotte
in partial fulfillment of the requirements
for the degree of Master of Science in
Mechanical Engineering

Charlotte

2019

Approved by:

_____
Dr. Christopher J. Evans

_____
Dr. Harish Cherukuri

_____
Dr. Edward Morse

ABSTRACT

CLARK HOVIS. Optical Metrology of Freeform Optics Utilizing Interferometric Stitching. (Under the direction of DR. CHRISTOPHER J. EVANS)

The utilization of interferometric stitching with coherence scanning interferometers has allowed these instruments to measure much larger areas than a single site measurement would permit. This has a major impact on the measurement of mid-spatials and form for freeform optics, which is hard or impossible through traditional means. The local slopes of these freeforms lead to non-null fringe measurements. These non-null measurements cause aberrations that are known as retrace errors. Minor retrace errors can influence stitching, which create form and mid-spatial errors that are orders of magnitude larger than the initial aberration. The aberrations caused by retrace errors can be calculated and corrected for. In this thesis, the stitching of a planar, mild freeform, and plano-convex optic are compared to a traditional technique: Fizeau interferometry. Retrace errors for coherence scanning interferometry based on non-null measurement is experimentally quantified. This information is then used to write a point by point correction in MATLAB based on local slope. The correction is implemented and assessed on a full stitch of a freeform optic. Finally, this thesis will explore expanding this process to other coherence scanning interferometers as well as other freeform and aspheric optics.

DEDICATION

I would like to dedicate this work to: my father, he has been training me since birth to be an engineer, without him this would not be possible; my mother, she has always been there for me and will always have a great stress relief technique; my sister, who understands the struggle of engineering graduate school, and knows when it is time for an inspirational speech and when it is time for a drink; Natalie Santibanez, she was the one who helped get me to go to graduate school and has pushed me to do my best since, without her love and support none of this would have happened. I would like to thank my family for the support emotionally and financially that made all this possible. I would also like to dedicate this work to the dogs – Couch Potato 'Chip', Rebel, Riley, and Bobo – that have helped prevent a mental breakdown through this endeavor.

ACKNOWLEDGMENTS

I would like to express my sincere gratitude to my mentor and thesis advisor, Dr. Christopher J. Evans, because without his guidance and support this thesis wouldn't be possible, and I would not be where I am today without his help. I would like to thank Dr. Hossein Shahinian for his help with the code, training me to use Fizeau Interferometers and Coherence Scanning Interferometers, and the countless conversation that gave me insight and understanding of optics. I would like to extend my thanks to Zach Reese, Prithiviraj Shanmugam, and Nicholas Sizemore for help and discussions about metrology and CSI stitching. I would like to thank Todd Noste for his help in machining the carriages. I thank Greg Caskey for acquiring one of the freeform stitches. I am also thankful to NASA for allowing me use their CSI and diamond turned optics to expand the correction. Finally, I would like to thank the Center of Freeform Optics for the financial support that without this thesis would not have been possible.

TABLE OF CONTENTS

LIST OF TABLES

LIST OF FIGURES

LIST OF ABBREVIATIONS

CSI	Coherence Scanning Interferometer
NA	Numerical Aperture
CNC	Computer Numerically Controlled
FOV	Field of View
MRF	Magnetorheological Finishing
NaN	Not-a-Number
FFT	Fast Fourier Transform
RMS	Root Mean Square
PSD	Power Spectral Density
PV	Peak to Valley
SPDT	Single Point Diamond Turning
MSF	Mid-Spatial Frequencies
NASA	National Aeronautics and Space Administration
IRAD	Internal Research and Development

CHAPTER 1: BACKGROUND AND MOTIVATION

1.1 Stitching

Surfaces with widely different topographies have been measured by stitching on a coherence scanning interferometer (CSI) [1] and those results compared with data from full aperture measurements. Stitching interferometry has been widely used in the optics metrology industry for the past decade, but the technology has been in use for a much longer period. Early interferometric stitching was used mainly as a method to expand the measured area of a surface. While this expanded the data maps, these early stitching methods were only able to measure low order form deviations as adjacent sites overlapped minimally (if at all) and were stitched together using a polynomial fit [2, 3]. Years later, the development of pixel based stitching greatly pushed this technology forward. Overlapping larger portions of adjacent sites allowed for, not only greater lateral stitching capabilities, but also increased ability to measure surfaces with large departures [4].

Stitching on a CSI today involves taking multiple measurements that are adjacent and overlapping. These measurements generally have a set overlap percentage of 20%. Once the individual sites are acquired, the measurements are processed through an algorithm that aligns each site and combines the overlap region. After the individual sites are combined, the result is a stitch. This method is mainly used for the measurement of freeform and aspherical optics, where measuring such optics with conventional interferometer setups are very limited. The high magnification of CSI objectives enhances the lateral and slope of the measurements significantly. This specifically has

potential in the rapidly growing field of freeform optics, which poses many metrology challenges. For freeforms, the measurements are generally required over relatively large lateral scales where there may be high slopes. Non-contact measurement of high slopes can be achieved using a high NA (or high magnification) interferometric objective, requiring stitching. CSI, may be a viable solution [5-7].

1.2 Freeforms

Freeform optics have revolutionized the forefront of research in the optics community. This group of optics have enhanced the design space of optical systems significantly. Compact optical systems with lower aberrations are achievable with such optics. While the manufacturing techniques for such geometries span from ultra-precise machining [8] to sub-aperture CNC polishing [9], the metrology solutions available for freeforms can be grouped to contact and non-contact measurement techniques. A full aperture interferometer setup for freeforms is not always a financially feasible approach. Instrumentation that provide a range of measurements for freeform optics tend to rely on sub-aperture stitching [10, 3].

1.3 Errors from Stitching

As studied in the past, non-null interferometric measurements, using conventional laser Fizeau interferometers, produce erroneous measurement data that could bias the reported residual surface errors on the optic [11, 12, 13]. The same issue arises in CSI of smooth optical surfaces [13]. For normal roughness measurements this may not pose a serious problem as the induced measurement artifacts may be removed by filtering and polynomial fitting following ISO standards. The problem can become of important when

stitching multiple CSI measurements to estimate mild freeform/aspherical mid-spatial frequency or form errors. These mid to low order errors are otherwise hard or impossible to measure without the CSI stitching.

Due to the varying slopes across one measurement zone of freeforms and aspheres, the null measurement of such areas is not achievable. The high density of fringes present in the measurement zone can give rise to errors and artifacts that can greatly skew the full aperture measurement post the stitching operation. The uncertainties in interferometric measurements due to the presence of fringes on the imaging system of the interferometer initially came to the spotlight during the measurement of aspherical optics with low departure from sphericity [14, 12, 15]. Evans and Bryan have investigated the errors produced in measuring optical components under non-null conditions in a laser Fizeau interferometer [11]. They show that the existence of dense fringes in the measurement of planar and spherical samples, were respectively dominated by comatic and spherical aberrations in the measurement. The extent of the errors is found to be directly correlated to the fringe density in the non-null measurement setup.

These small retrace errors in the measurement can lead to induced aberrations in the form and mid-spatials post stitching, which are orders of magnitude larger. It has been demonstrated in literature that the retrace errors can be corrected for a CSI [16, 17].

The concepts of stitching, retrace errors due to non-null measurements, and correction of the errors, which are outlined in this chapter, will be experimentally explored and assessed in the following chapters.

CHAPTER 2: TESTING AND COMPARING STITCHING WITH CSI

2.1 Introduction

This chapter's goal was to utilize interferometric stitching to measure from form to roughness in a single data set. Then use the stitch to compare to a reference measurement taken from a laser Fizeau interferometer. Dominant uncertainties in the Fizeau measurement of form (considered here as the departure from nominal shape of the reference surface – after removal of rigid body terms – for lateral scales from full aperture to 10 cycles/aperture) are (a) reference surface departure from nominal; (b) retrace errors; and (c) time varying measurement noise arising mostly from electronics noise and in cavity turbulence. Over the apertures of parts discussed here, the order of magnitude of these contributions are:

(a) 10 nm PV;

(b) <20 nm PV; and

(c) ~3 nm rms

for the measurements made with transmission flats (sections 2.2.1 and 2.2.2 below). For the measurements using the transmission sphere (Section 2.2.3 below) item (b) above will be of order 20% higher and item (c) ~2x larger because of the longer air cavity. These uncertainty contribution are uncorrelated and insignificant compared to the bias reported in Section 2.4.

The uncertainty in matching tip/tilt, slope, and curvature in the overlap region of the stitch could lead to bias in the measurement of low order form. In some cases, this bias could propagate through the measurement and be amplified as the number of patches

stitched increases. The purpose of the work described in this chapter was to evaluate the stitching process in a commercially available CSI instrument when looking at form, mid-spatail error, and roughness evaluated in a single set-up. A planar (nominally flat), freeform surface that departs from a flat, and the spherical surface of a plano-convex lens are all tested [18].

2.2 Experimental Setup

2.2.1 Planar Optic

The first sample used was an optically polished BK7 glass flat with a Ø40 mm. The optic was mounted in a polycarbonate carrier, made on a Haas TM1 CNC machine, to allow easy fixturing in a variety of instruments with minimal concerns about mounting induced deformation as the section thickness of the carrier was much greater than the thickness of samples. The sample was first measured on a Zygo Verifire Fizeau interferometer using a transmission flat to obtain a reference measurement to compare to the CSI stitching results [19]. Next, the sample was moved to the CSI instrument for stitching. A stitch was taken over the entire aperture of the sample on the Zygo NexView CSI using the 2.75x objective with a 1.0x tube (3 mm x 3mm FOV). Three different overlap percentages were used, 10%, 20%, and 30%. Note that as the percent overlap increases, so does the number of sites required for full coverage and the measurement time.

TABLE 2-1. Overlap percentage affect on sites and time.

Overlap Percentage	Number of Sites	Time (minutes)
10 %	196	30
20 %	244	42
30 %	314	55

Each of the measurements were stitched with all four algorithm and three merge choices available in Mx, the software supplied with the instrument used. The algorithm options available were Adaptive Adjust, Cartesian, Overlay, and Adjust XY. The Cartesian algorithm adjusts each site with five degrees of freedom for alignment, Overlay aligns based on the stage coordinates of the instrument, and Adjust XY aligns with only two degrees of freedom. The merge choices available were Average, Blend, and No Merge. “Average” takes the average of the two measurements in the overlap, “Blend” does an interpolation in the overlap region, and No Merge does not merge the two measurements in the overlap region by choosing the measurement with the better quality data to use [20].

2.2.2 Optical Freeform

The next sample tested was a freeform that was manufactured at UNC Charlotte, based on a BK7 glass flat with a ∅40 mm. A QED MRF machine was used to make the freeform surface [21]. The part was created with astigmatic (quadratic, 2 cycles azimuthally) and comatic (cubic, one cycle azimuthally) components. Each component had a designed Zernike Fringe coefficient of approximately 3000 nm [22]. The clear

aperture of the optic was Ø35 mm. This freeform was designed to have mild enough sloped that it could be measured on the Fizeau interferometer. The optic was mounted in a polycarbonate carrier similar to that used for the planar optic. The carrier was also fitted with silicon nitride ball to transfer the coordinate system. The sample was then measured on a Zygo Verifire Fizeau interferometer using a transmission flat to obtain a reference measurement. After this measurement was obtained the sample was moved to the Zygo NexView CSI for the stitching measurement. A stitch of the full optic was acquired on the CSI instrument. For this stitch a 2.75x objective with a 0.5x tube lens was used, and the overlap percentage was set to 20%. Since this optic was a freeform there was varying fringe density at each measurement site in the stitch. This cannot be mediated by changing the tilt from site to site, because the stage is not parcentric at the optical surface, meaning that changing tilt introduces a lateral shear. This issue along with the slope limit of the objective was taken into consideration, and led to the fringes being nulled at the center of the optic with the scan range set long enough where all the features were captured. After the measurement was complete it was stitched together using all four algorithms and all three merge choices, similar to the planar part.

2.2.3 Convex Optic

The final optic used in this set of tests was a commercial grade plano-convex lens. The part had a Ø12 mm with a focal length of 84 mm. The optic was mounted in a polycarbonate carrier that was CNC machined. Similar to the previous optics it was first measured on a Zygo Verifire Fizeau interferometer. Since this optic was convex instead of planar or a mild freeform, a transmission sphere was used for the measurement. The

transmission sphere that was chosen for this measurement had an f# of 1.5 and a focal length of 154 mm. After the reference measurement was acquired the sample was moved to the Zygo NexView CSI for the stitching measurement. A 10x objective with a 1.0x tube lens was chosen (with a FOV per measurement site of approximately 0.8 mm x 0.8 mm). The higher slopes of the convex part needed a higher magnification and NA to be within the slope limit of the objective. Similar to the freeform optic there was varying fringe density in each site and over the whole stitch, since the stage of the instrument was not parcentric. To attempt to minimize this the fringes were nulled at the apex of the lens, and the scan range was set long enough to capture the entire height of the lens. The stitch overlap was set to 20%, and the measurement went through all algorithm and merge choices.

2.3 Data Processing

Raw data acquired and stitched in Mx were acquired and exported to MATLAB to ensure full control of data processing. Each data set was processed using the same sequence except where explicitly stated. The first step was to crop and mask the data to the desired diameter. The planar and convex parts were cropped to Ø38.45 mm and Ø11.6 mm respectively. This was done to remove the edge effects, such as diffraction, from the measurement. The freeform was cropped to Ø35 mm, the clear aperture of the optic. Then piston and tip/tilt were removed from the measurements, as these are errors inherent in the setup. For the convex optic the power was also removed. Next a linear interpolation was done to fill the NaNs within the cropped part diameter. This process was performed to prevent the NaNs from affecting the Fourier filtering and the statistical calculations. A

filter was then applied to the data. The filter chosen was a FFT high pass filter with a 0.2 mm period cutoff. This cutoff was chosen so the CSI stitching data could be appropriately compared to the Fizeau data.

After the filter was applied, the CSI stitching data matrix was interpolated down to the size of the Fizeau data matrix. This created data with the same lateral resolution, and allowed for the CSI stitching data to be easily compared to the Fizeau data. The S_q (area RMS) was calculated, in accordance with ISO 25178-2, for each CSI stitch, and each Fizeau measurement [23]. Each of the CSI stitching measurements were then subtracted from their respective Fizeau measurement, and the S_q of the subtraction was calculated for each. Then to assess how consistent the form data was for each measurement, the Zernike polynomials were calculated through sixth order for rotationally varying and rotationally invariant terms.

Lastly, the frequency content of the measurements was evaluated. This was done by calculating the average 1-D PSD for each measurement. To do this 360 radial profiles were taken from each measurement, one for each degree azimuth. For each profile the PSD was calculated following Church's rule and using a uniform window. Then each of the PSD profiles were averaged together to get the average PSD of the surface.

2.4 Results and Analysis

The reference measurements that were completed on the Fizeau interferometer for each optic are shown below in Figure 2-1.

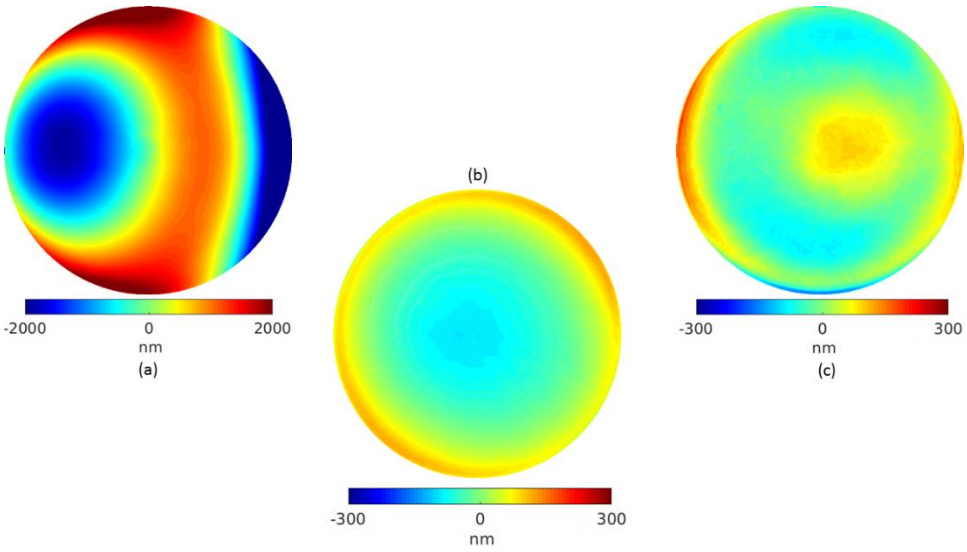

FIGURE 2-1: Reference Measurements completed on the Fizeau.
(a) Freeform with piston and tip/tilt removed
(b) Planar with piston and tip/tilt removed
(c) Convex with piston, tip/tilt, and power removed

The RMS of the subtraction (called $S_q\Delta$ hereafter) from the Fizeau and CSI measurements for the planar optic are shown in Figure 2-2. The $S_q\Delta$ for the 20% overlap are the lowest of the three overlap percentages used. Initially this seems counter intuitive because a higher overlap percentage should mean lower uncertainty in the stitch, but at the cost of longer data acquisition times. This argument may explain the modest improvement when increasing from 10% to 20% overlap. The large increase in the 30% overlap stitches may be explained by a quadratic bias in the reference surface (see Chapter 4).

The overlay algorithm, for all three merge choices, were much higher than any of the other algorithm and merge combinations. Ignoring the overlay results, the rest of the algorithms agreed within 2 nm of each other for the same overlap percentage.

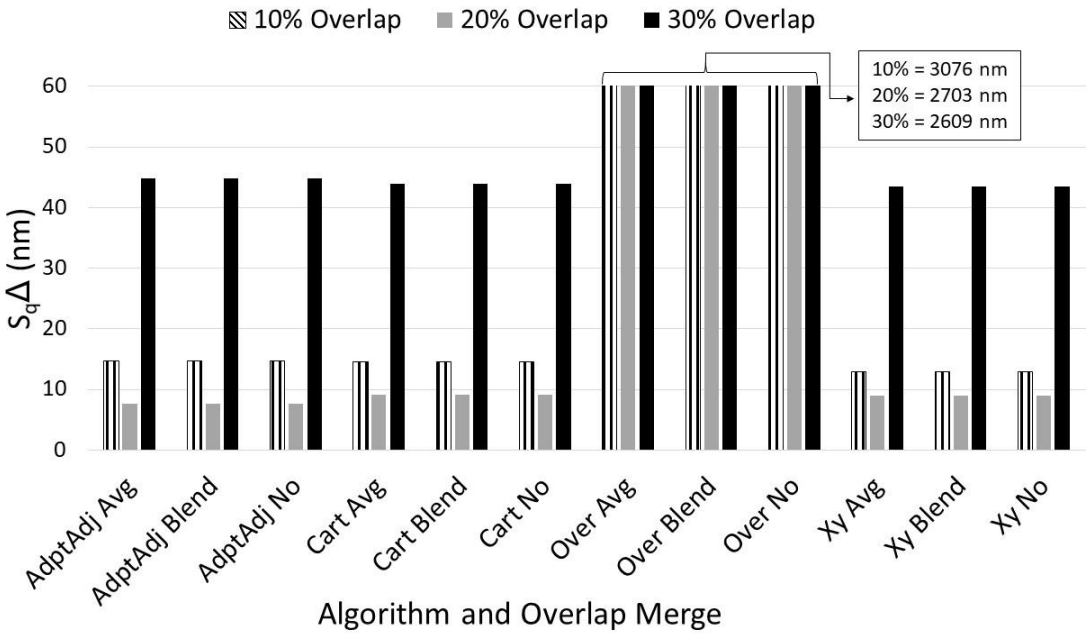

FIGURE 2-2: Planar Optic $S_q\Delta$ results for all algorithms, merges, and overlap percentages.

The results for the freeform had similarities to the results of the planar optic. The overlay algorithm had a much higher $S_q\Delta$ than any of the other algorithms. The other algorithms were all within 8 nm of each other. One major difference between the planar and freeform optic were the much higher $S_q\Delta$. Each of the $S_q\Delta$ were over 300 nm. Figure 2-3 shows the $S_q\Delta$ for the freeform. These results were higher than should be expected from retrace errors in the Fizeau, due to non-null measurement, and the bias in the transmission flat. Deck (2007) briefly described a correction of retrace errors in a custom CSI [17]. A different approach to correcting retrace errors caused by non-null measurements, which drive this higher $S_q\Delta$, is described in Chapter 3.

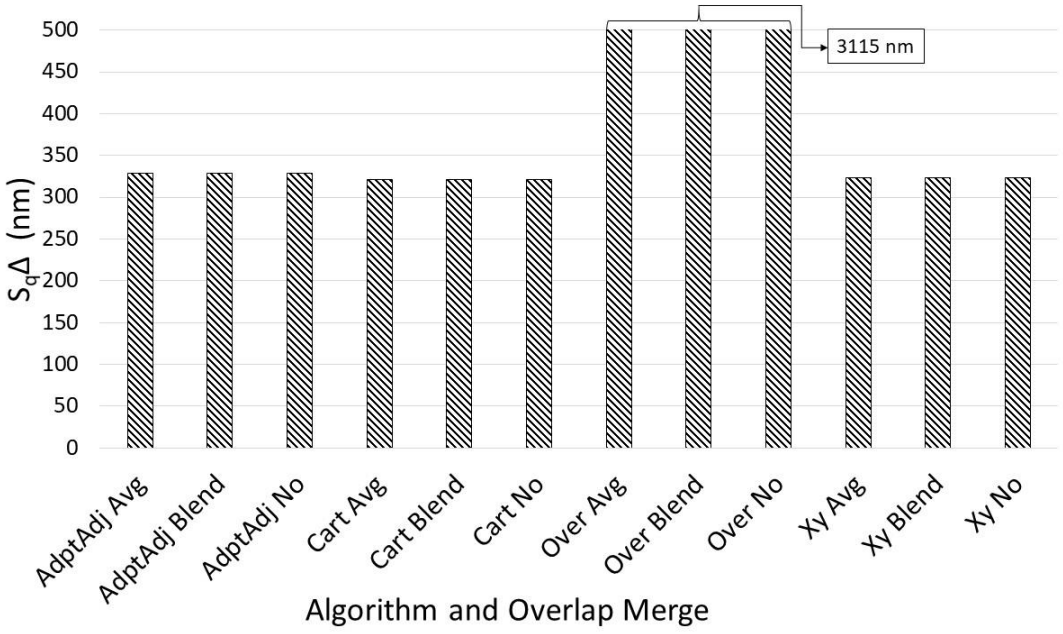

FIGURE 2-3: Freeform Optic $S_q\Delta$ results for all algorithm and merge choices.

In Figure 2-4 it shows the $S_q\Delta$ for the convex measurements. The convex optic results were slightly different than the previous two optics. Similarly, outside of the overlay algorithm the $S_q\Delta$ were within 15 nm of each other. The $S_q\Delta$ were higher for all the algorithms, other than overlay, when compared to the planar and freeform optic. The overlay algorithm, however, was lower than all the other algorithms on the convex part, and was lower than the overlay results for the planar and freeform optic. The way that the overlay algorithm works, based on stage coordinates, could have caused this because the retrace errors from the CSI would not affect the alignment of the sites for the stitch.

A number of factors may have contributed to the relatively large SqΔ values. The slopes and number of sites are larger which is expected to give larger retrace errors that propagate and amplify. Also, the Fizeau measurement using a transmission sphere reports

normal departure from a best fit spherical cap while the CSI reports deviations parallel to the optical axis.

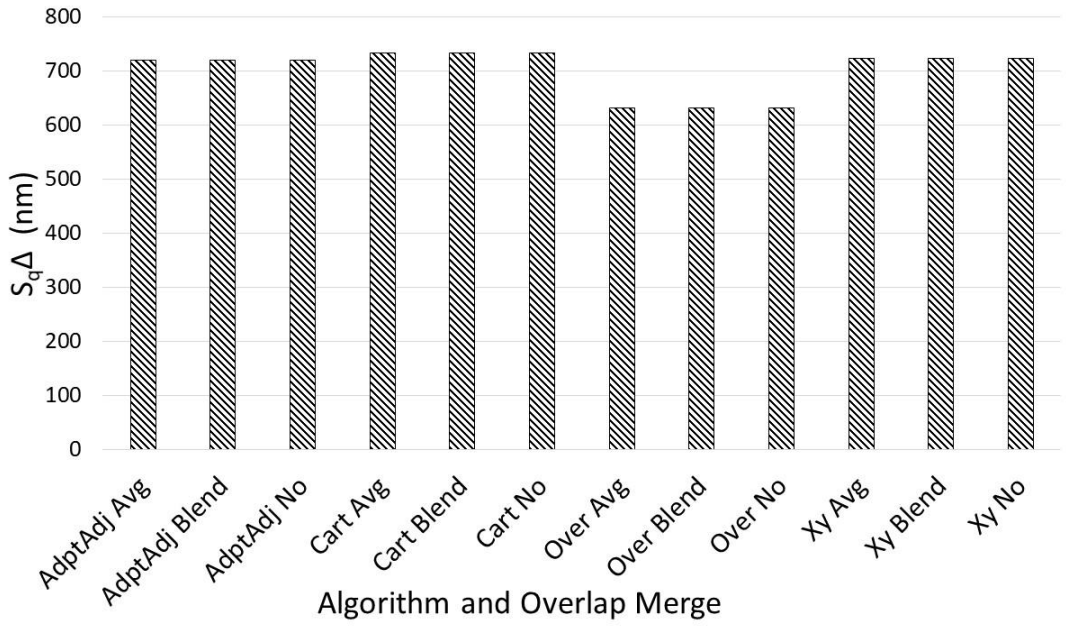

FIGURE 2-4: Convex Optic $S_q\Delta$ results for all algorithm and merge choices.

The Zernike coefficient calculations showed what was expected from the $S_q\Delta$ results. Outside of the overlay algorithm, results for the planar part were within 13 nm of the Fizeau. For the freeform part, the Zernikes deviated by 51-82 nm compared to the Fizeau, but were within 31 nm of each other. Similar to the $S_q\Delta$ results for the convex optic, the overlay was closest to the Fizeau with a difference of 107 nm. The deviations for the other convex algorithms were greater, 246-270 nm. Discrepancies between the Zernike coefficient calculation and the $S_q\Delta$ calculation were attributed to the way the subtractions were calculated, and that the Zernike coefficients were only calculated through the sixth order.

Figure 2-5 through 2-7 shows the PSD results for the planar optic at 10%, 20%, and 30% overlap respectively, and the reference measurement. The average merge was the only one plotted because the results for the same algorithm, but different merge, were indistinguishable in the plot.

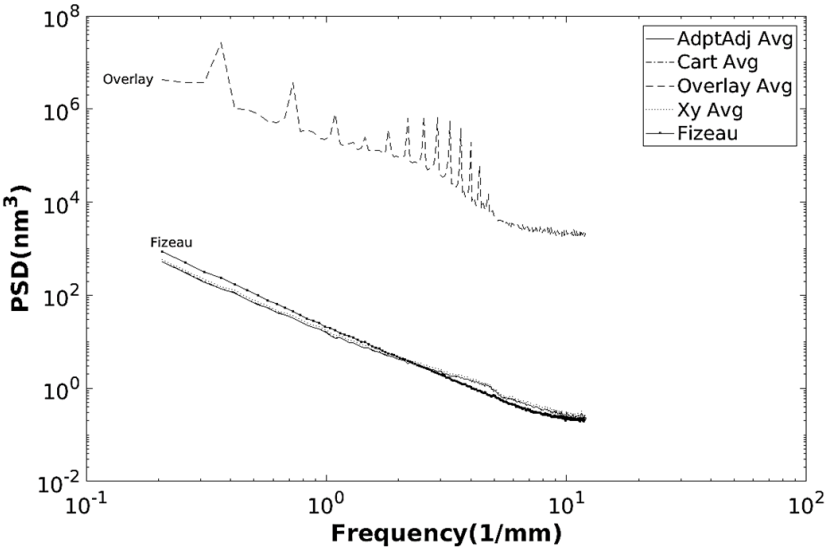

FIGURE 2-5: Average PSD graph for the planar part with 10% overlap and the Fizeau.

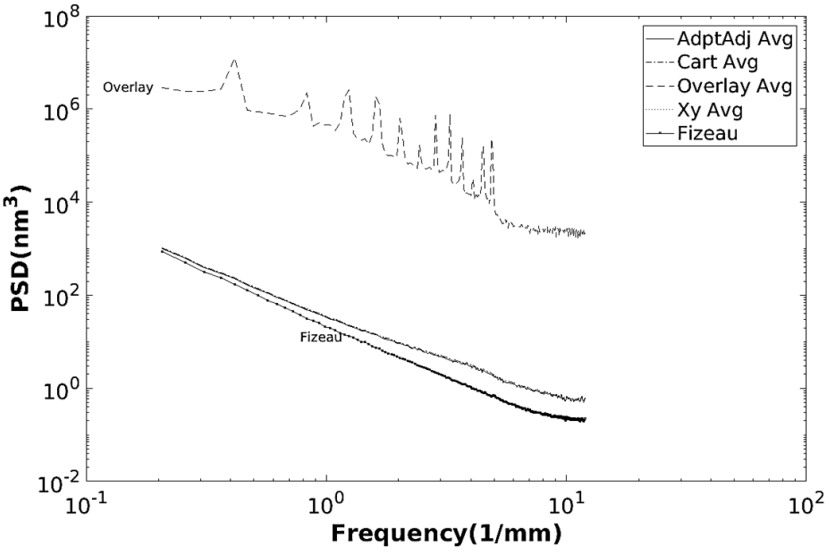

FIGURE 2-6: Average PSD graph for the planar part with 20% overlap and the Fizeau.

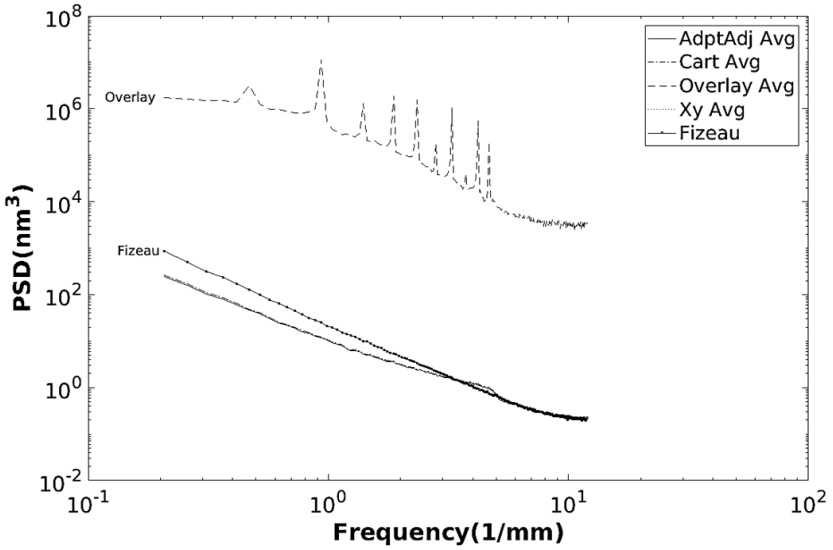

FIGURE 2-7: Average PSD graph for the planar part with 30% overlap and the Fizeau.

Similar to the $S_q\Delta$, the PSD for the overlay algorithm was different than the results of the other algorithms. The spikes in the peaks on the overlay algorithm were caused by stitching artefacts in the measurement. These artefacts occurred where the profile extracted crosses in between stitching sites. Since these profiles were taken at different azimuth angles, the different distances the profiles take across each stitching site overlap region correlate to the spikes in the overlay algorithm. Results for the other algorithms, were consistent with the results that were seen with the $S_q\Delta$. The 20% overlap was the closest to the reference measurement in the lower frequencies, which led to the smallest $S_q\Delta$ because the lower frequency deviations had a greater effect than the higher frequency deviations on the $S_q\Delta$. This affect occurs due to the fact that the RMS is equal to the area under the PSD curve. This was also shown in the 30%, which had the lowest deviation in the lower frequencies, the highest deviation in the higher frequencies, and had the largest $S_q\Delta$.

The PSD results for the freeform optic are in Figure 2-8. Similar to the planar optic, the overlay algorithm had the highest deviation from the Fizeau, and the stitching artefacts were still present. The other algorithms were close to the reference in the lower frequencies, but deviated greatly at the lower frequencies especially after the spike at 0.4 1/mm. This spike was believed to be a feature created by the MRF process.

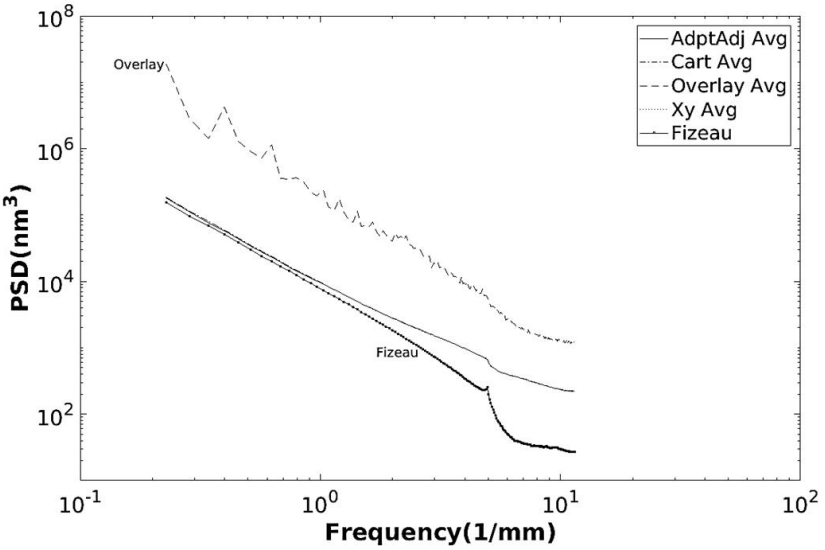

FIGURE 2-8: Average PSD graph for the freeform part and the Fizeau.

The convex optic results, which can be seen in Figure 2-9, showed that, unlike the previous results the overlay algorithm, was in line with the other algorithms. but there were still some stitching artefacts present. The stitching artefacts, however, were not as prevalent as they were in the planar measurements. The PSD plot also showed that, outside of the three stitching artefacts, it was the closest algorithm to the Fizeau reference measurement. This result was consistent with what was shown with the $S_q\Delta$.

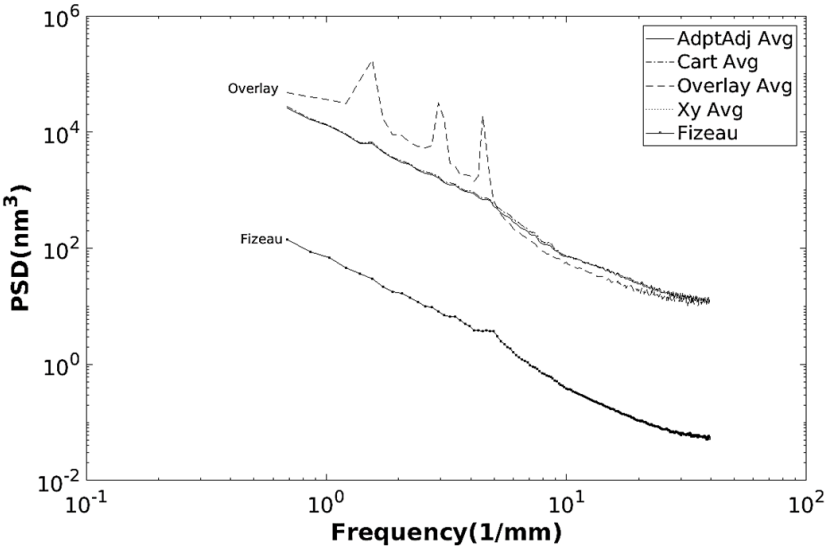

FIGURE 2-9: Average PSD graph for the convex part and the Fizeau.

CHAPTER 3: RETRACE ERROR AND CORRECTION

3.1 Retrace Errors

The previous chapter showed that errors arise in the CSI when the measurement was taken under non-null conditions. It has also been shown that non-null interferometric measurements using laser Fizeau and other interferometers produce erroneous measurement data that could bias the reported residual surface errors on the optic [11, 12, 13]. Evans and Bryan have investigated this phenomena, and shown experimentally that the existence of dense fringes in the measurement of planar and spherical samples results in systematic measurement errors [11]. Comatic, for tilt errors, and third order spherical aberrations for power errors are dominant in these measurements. Grievenkamp et al have considered this problem theoretically based on an assumed optical design of the Fizeau interferometer [15]. Deck and Evans (2005) and Deck (2007) have given brief descriptions of the bias resulting for retrace errors in a custom CSI system making single FOV measurements on surfaces with varying fringe density [13, 16]. As indicated in Chapter 2, errors in single fields of view may propagate non-linearly in stitching applications.

3.1.1 Retrace Error Effect Simulation

To demonstrate the effect of measurement artifacts from stitching, simulated measurement data with coma values of 5 nm PV were generated. To do the simulation two panels in the Y direction and five panels in the X direction were created. The fake data was then stitched using the algorithm and merge choice Cartesian blend. Figure 3-1 shows the result of the stitching of the measurements with the simulated comatic errors.

The stitched results showed a mid-spatial component with a S_q of 1.2 nm and a 9.7 nm PV. This was almost twice as large as the simulated retrace error in each of the input panels. The result clearly demonstrates the advantage of minimizing the effect of the retrace error on each measurement panel in the final stitched result.

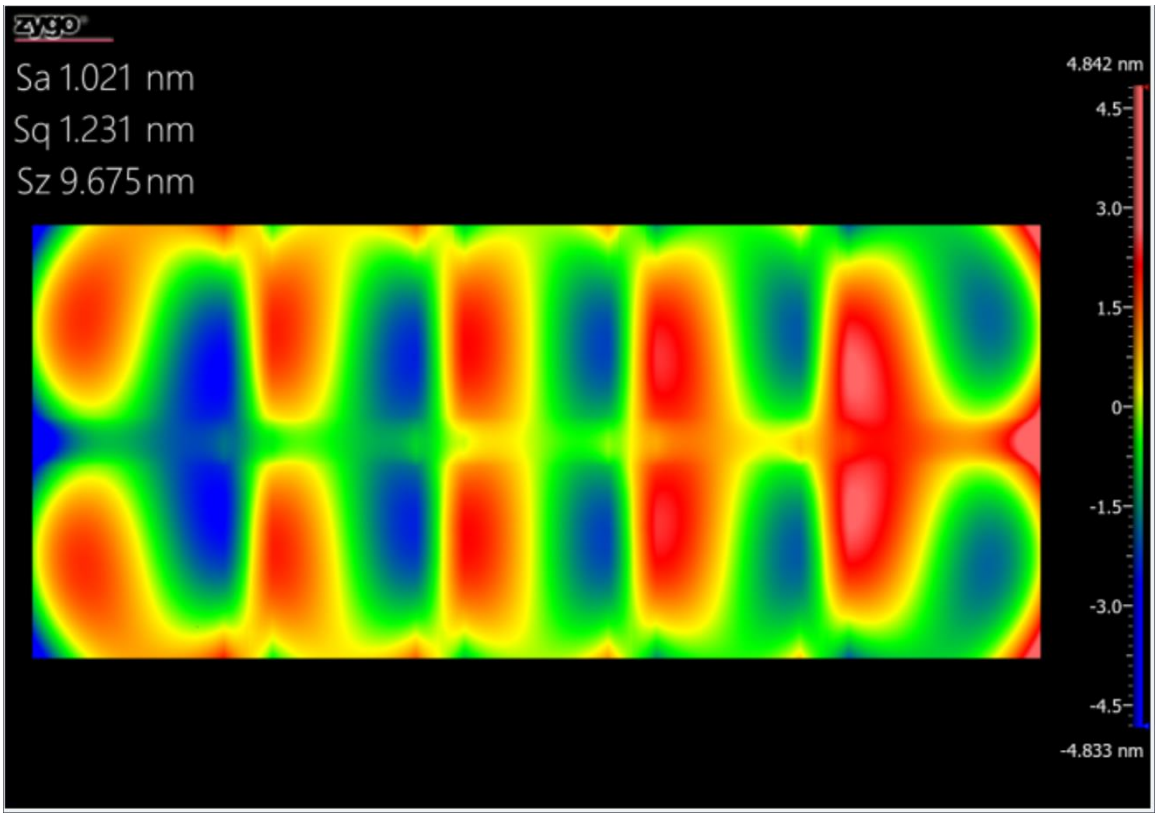

FIGURE 3-1: Stitching outcome from panels with simulated coma.

3.1.2 Measurement of Retrace Errors in CSI

To quantify the aberrations induced caused by a CSI measurement under non-null conditions, a silicon carbide flat was measured on the Zygo NexView CSI with a 2.75x objective and a 1x tube lens. The non-null data was acquired by tilting the sample at 0.25º increments, which was programmed into the stage, in two orthogonal directions. Figure 3-2 shows a sample of the progression of the aberrations observed (after removal of tilt)

as tilt is increased in one direction. The measurement results are dominated by a comatic error. The magnitude of the coma increased as the fringe density, or tilt, increased in the measurement.

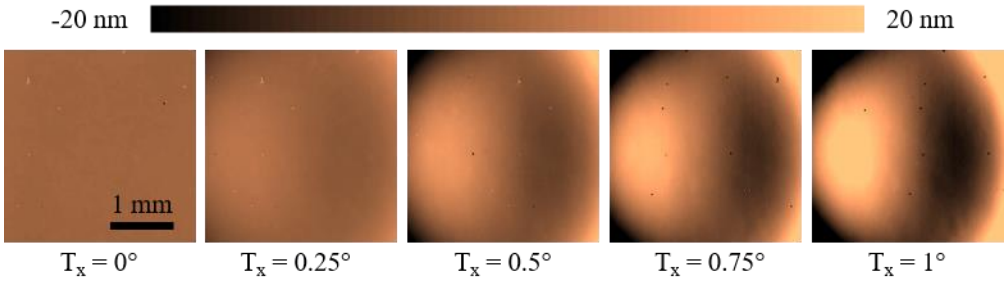

FIGURE 3-2: Aberration artifacts induced by non-null fringe density in CSI measurements of a polished silicon carbide flat.

To quantitatively evaluate these errors, a decomposition of the measurement data using orthonormal based polynomials was used. Chebyshev polynomials were chosen, rather than Zernikes for two reasons:

(a) The CSI instrument has a square aperture for which Chebyshev polynomials are an orthogonal representation across the used; and

(b) Both extrapolating from Zernike fits on an inscribed circle and fitting Zernikes to the square aperture where the normalization radius was half the diagonal gave worse correction results than described below.

3.2 Correction of Retrace Error

The correction method outlined here was written and implemented in MATLAB.

3.2.1 Correction Method

The efforts were primarily focused on point by point algorithmic correction of CSI measurements based on the experimental data obtained and outlined in 3.1.2. To

create the correction function, the measurements data at each tilt was decomposed using Chebyshev polynomials to 6^{th} order. The produced fit of Chebyshev data served as a predictive model of the amount of retrace error at any point in the aperture as a function of the fringe density (local slope) of that point.

Local gradients were calculated using a 5-point finite difference scheme. This scheme has an error of the 4^{th} order of the data spacing. The scheme was implemented in both X and Y. Near the boundaries of the measurement area a linear extrapolation was applied for the two points that did not exist for the gradient calculation.

The value of the expected induced retrace error at each point in the measurement was calculated based on the position in the aperture and the slope of the point. The corrected value was calculated by subtracting the calculated retrace error from the measurement.

3.2.2 Preliminary Test of Correction

For a preliminary test of the outlined correction method, the same silicon carbide flat used to generate the correction was tilted in a direction between the orthogonal directions used in 3.1.2, and data was acquired. The measurements exhibited the expected coma dominated artifacts. The results after the correction method are shown in Figure 3-3. The correction clearly decreases the deviation, and comatic errors, between the measured data and the expectation. At relatively large tilt, however, the correction left a detectable deviation which appears to be dominated by a high order astigmatism at 45 degrees (ie high point at diagonally opposite corners of the aperture). In addition there is

a faintly visible ripple orthogonal to the tilt direction which may be the consequence of vibration or camera non-linearity.

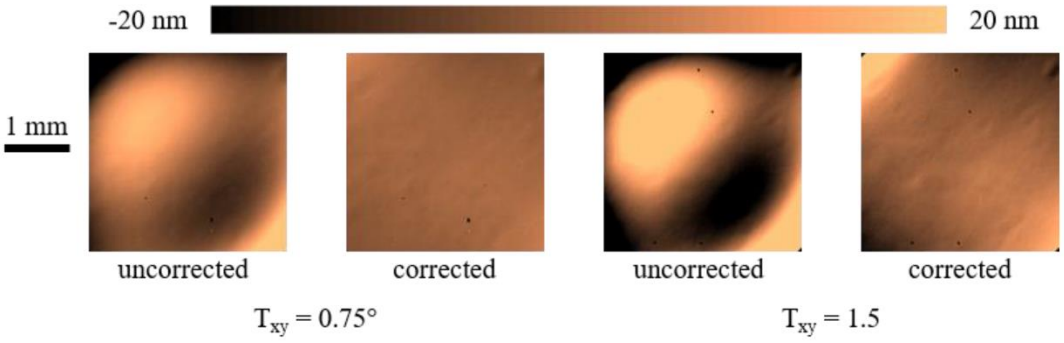

FIGURE 3-3: Implementation of the correction in MATLAB to CSI measurements at XY tilted silicon carbide sample.

3.2.3 Implementation of Correction on a Full Stitch

The freeform optic from Chapter 2 was used to test the correction on a full stitch. The 2.75x objective with a 1x tube lens (3 mm x 3 mm FOV) was used to acquire a full stitch of the freeform. Each site that had any of edge of the optic was completely removed. This was to prevent edge effects, such as diffraction, from altering the slope calculations, and in turn the correction. Then each of the sites were processed through the correction. After the correction was implemented, the sites for both the corrected and uncorrected data were stitched together using the Adjust XY algorithm and the Blend overlap merge. The stitches were then cropped to Ø32.5 mm. Next, the data sets had a FFT high pass filter with a 0.2 mm period cutoff applied to them. Then both of the processes stitches were subtracted from the Fizeau reference measurement, and the $S_q\Delta$ was calculated.

3.2.3 Results and Analysis of Correction on Full Stitch

The results for the subtraction of the reference from the uncorrected data and the corrected data are shown in Figure 3-4 and Figure 3-5 respectively. The $S_q\Delta$ results are shown in Table 3-1.

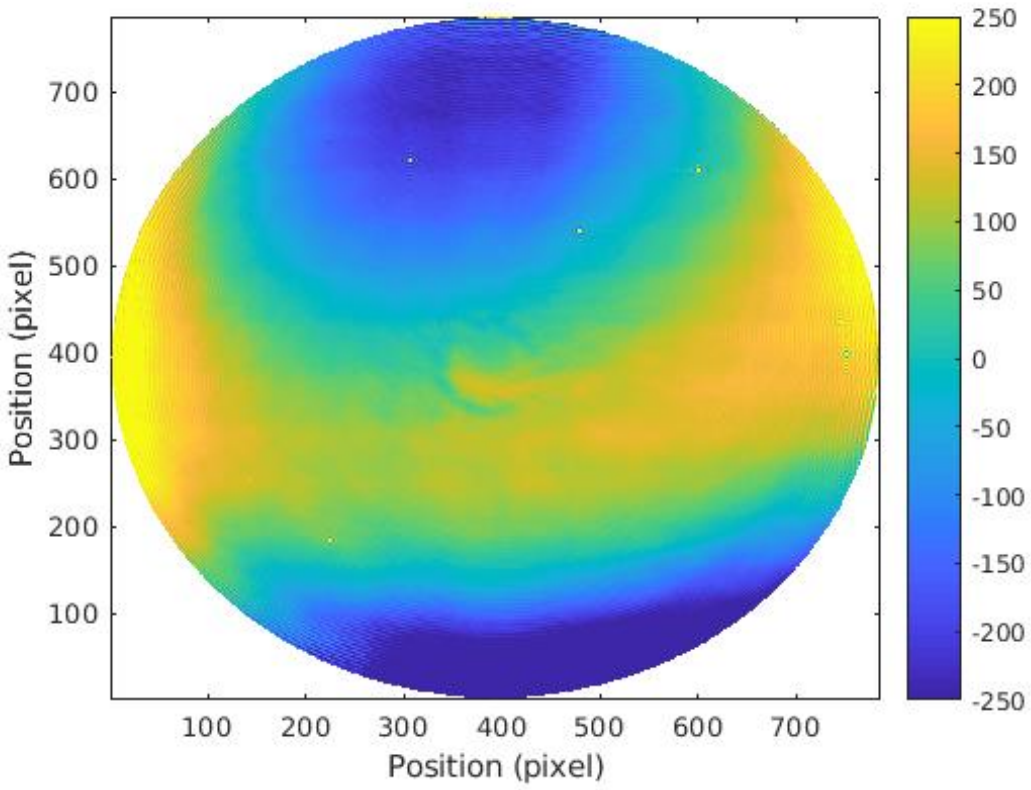

FIGURE 3-4: Δ map of uncorrected freeform stitch minus reference measurement.

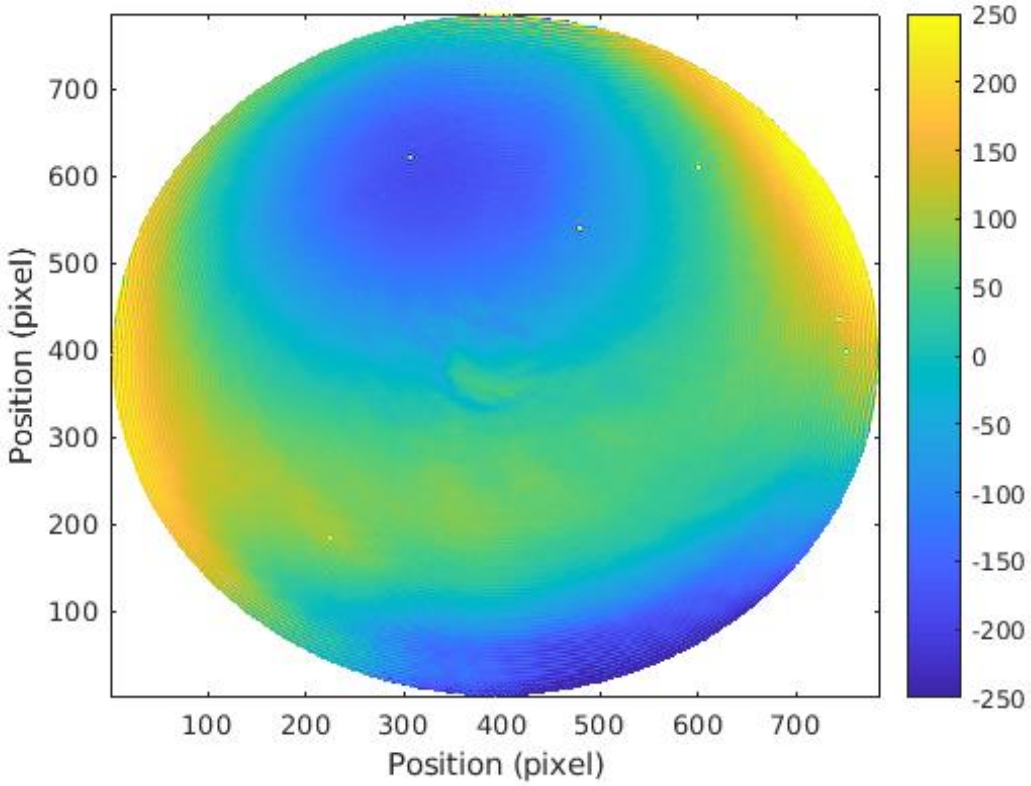

FIGURE 3-5: Δ map of corrected freeform stitch minus reference measurement.

TABLE 3-1. $S_q\Delta$ Results for uncorrected and corrected stitches.

	$S_q\Delta$ (nm)
Uncorrected	147.70
Corrected	101.06

The results showed a reduction of the $S_q\Delta$ of almost 47 nm after correction. In Figure 3-4 it can be seen that higher deviations from the reference measurement occur at the higher slopes which had higher fringe density during the measurement. Figure 3-5 shows that the correction noticeably reduced the error at these higher slopes. The subtraction map for the uncorrected data shows stitching artefacts, i.e. the “waffle pattern” seen in Figure 3-4. For the corrected data these stitching artefacts have been

removed. The correction, while promising, is imperfect. One reason could be errors in the fit of the Chebyshev data outlined in 3.2.1. Another could be a low order error in the reference optic for the CSI objective that propagates through the stitch. The idea of a low order error in the reference optic is explored in Chapter 4.

CHAPTER 4: SIMULATION OF REFERENCE ERROR

The retrace correction outlined in chapter 3.2.3, was imperfect. This could have been caused by an error in the reference optic for the CSI. To explore this effect a simulation of a reference error in a stitch was done.

4.1 Simulation Setup

For the simulation, the chosen reference error was a 2 nm PV Zernike fringe power term. The 2.75x objective is a Michelson interferometer with a relatively large reference surface (compared to the small references in the Mirau objectives). The manufacturer's guideline for an "acceptable" reference calibration is 2 nm. The most likely cause of a calibration change is a thermal effect or the result of humidity changes on the adhesives used in assembly. These changes are most likely quadratic.

The stitches simulated were a perfect 2x3 and 2x5 with no noise, spikes, or deviations. Each site in the stitch then had this reference error added. Figure 4-1 shows the simulated error for an individual site. Then the sites were stitched together using Adjust XY Blend. The way this simulation was setup should have resulted in a stitch that looked Figure 4-2 for the 2x5 stitch, and the same for the 2x3 stitch with the last two columns removed.

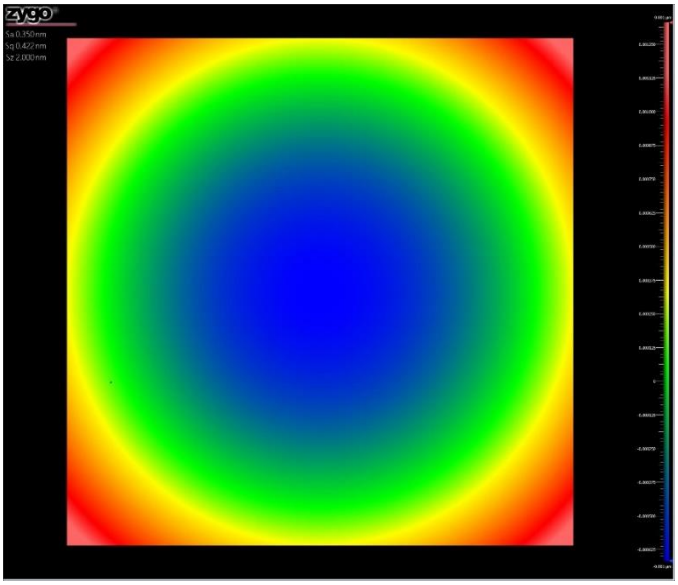

FIGURE 4-1: Simulated reference error, 2 nm PV of power.

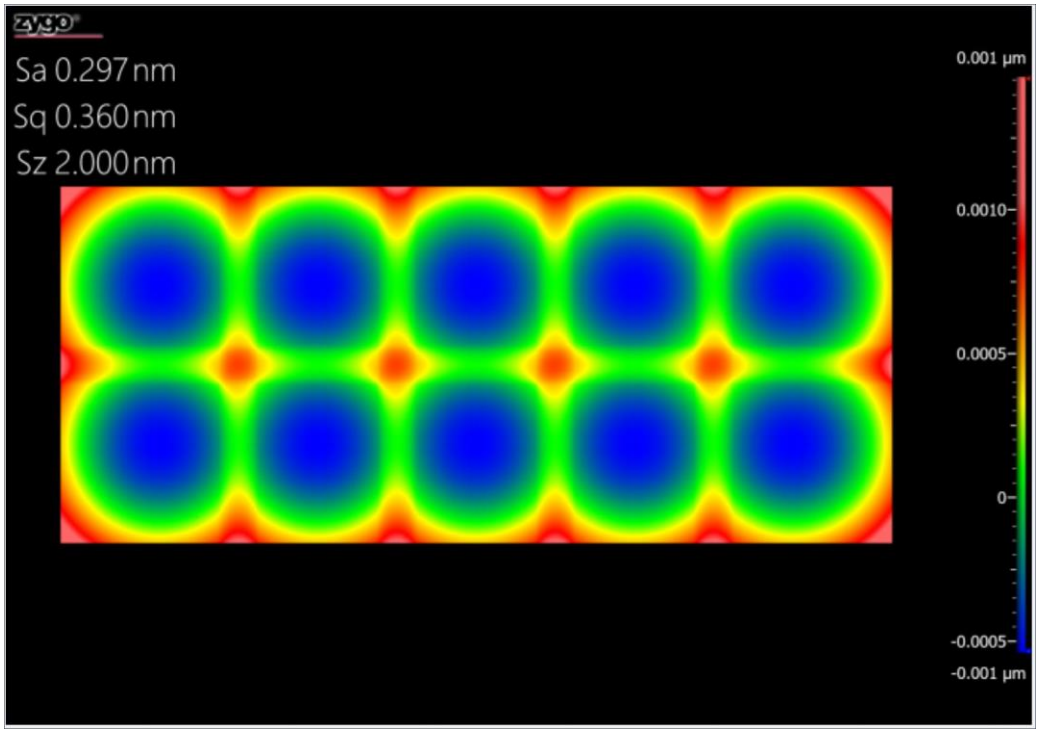

FIGURE 4-2: Theoretical simulation inputs.

4.2 Simulation Results and Analysis

The results for the 2x3 simulation is shown in Figure 4-3. Figure 4-4 shows the simulation results for the 2x5 stitch. The 2x3 stitch had a PV of 10 nm, and the 2x5 stitch had a PV of 21 nm. The 2 nm reference error gives an added 8 nm error in the 2x3 stitch and 19 nm in the 2x5. These results showed that the error propagates and is amplified non-linearly as the stitch gets larger. The results in Chapter 2 are based on a large number of stitched sites (approaching 350 for the convex optic). This also explained some of the imperfections within the correction described in Section 3.2, since that correction was only attempting to correct for non-null fringe density and not for reference errors.

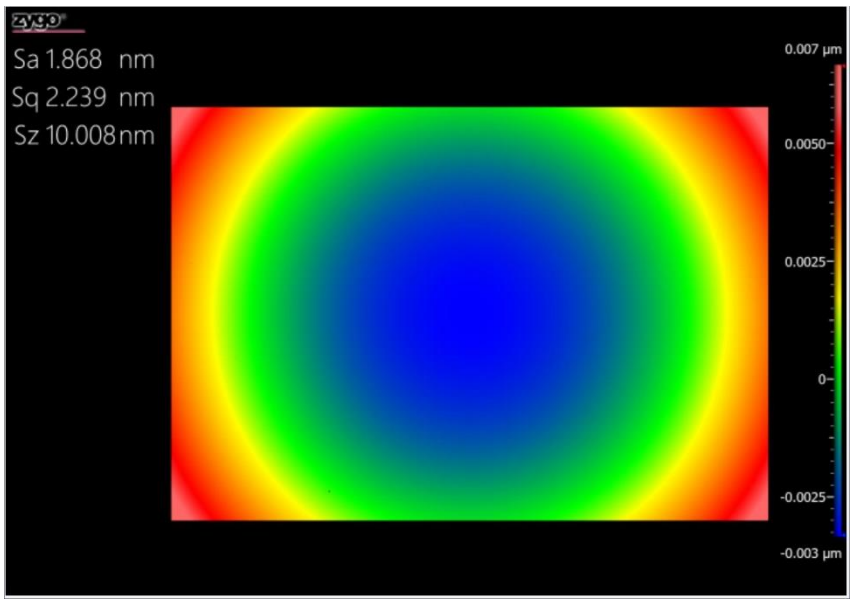

FIGURE 4-3: 2x3 simulation of reference error.

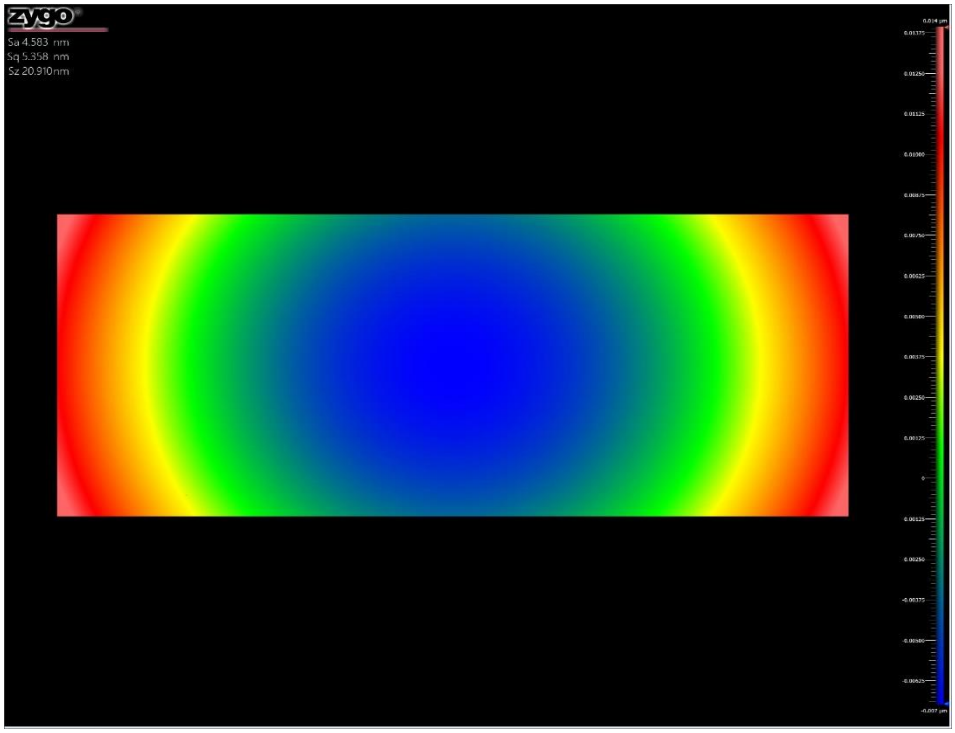

FIGURE 4-4: 2x5 simulation of reference error.

CHAPTER 5: CORRECTION OF DIAMOND TURNED OPTICS

In the previous chapters, the correction method was applied to polished optics. Single point diamond turning (SPDT) is used to produce aspheric and freeform optics. Depending on the specifics of the particular process, the surface may have both two periodic structures. The shorter wavelength structure is the cusp structure from the feed per revolution of the spindle; a longer period, referred to as a "mid spatial frequency" (MSF) in optics and waviness elsewhere, arises in SPDT from leadscrew errors and roller pass frequencies in older diamond turning machines and from thermal cycling of the main spindle in fast- and slow- servo turning on more modern machines. These MSF on aspheric and freeform optics may have periods of order 1-2 mm but will likely be super-imposed on surfaces with large enough slopes that higher NA, smaller field of view objectives will be required; this implies that stitching will be required.

In this chapter preliminary evaluations of the correction method when measuring such diamond turned surfaces are reported. The preliminary results point to areas where further work is required.

5.1 Freeform Optic from NASA PENTA IRAD

This portion of the work was done at NASA Goddard Space Flight Center in conjunction with the PENTA IRAD project. This test was done to look specifically at the MSF of the optic under test, not the figure or roughness. The optic under test was a diamond turned aluminum freeform mirror, which was referred to as M1 for the PENTA IRAD project. Unlike the tests reported in previous chapters, there was no reference test for comparison. For comparison, the MATLAB based correction described earlier was

compared with a process in which aberrations in each site were removed before stitching. In this method each stitch site had the Zernikes up to 6^{th} order removed from the data before stitching. This approach is much easier and quicker to complete (using the commercial software supplied with the CSI) than the MATLAB based correction. Also since the goal was to look at the mid-spatials, and not the form, removing the form Zernikes might have a minor effect on MSF, although a priori this is difficult to evaluate without knowing the frequencies involved and the FOV required for the measurement. The Zernike removal may attenuate MSF of interest.

5.1.1 Experimental Method

To perform this optical test a Zygo NewView 8300 CSI with a 5.5x objective and a 0.5x tube lens was used (3 mm x 3 mm FOV). The first step was to find how the fringe density influences coma and other aberrations. This was done as described in chapter 3. A super-polished silicon carbide flat was placed on the instrument, and a measurement was taken at the null fringe. After this was done, the sample was tilted in the X direction, and another measurement was completed. This was repeated until 15 measurements were done. The sample was then moved back to the null fringe, and the process was repeated for the Y direction. After the Y direction, the sample was then returned to the null fringe, and the process was done again, but for a combination of X and Y to get the cross term. For the XY test 10 measurements were taken. Once the data for the varying fringe density was acquired, it was put into a MATLAB code that calculated the relationship of fringe density to different Zernike terms up to the 6^{th} order. Note the earlier comments about orthogonality of Zernikes on non-circular apertures.

The next step was to perform a stitch on the M1 optic. The measurement was a sub-aperture stitch of the optic, which had 49 sites (7x7) near the center of the optic with a 20% overlap. The three data sets raw, Zernike removed, and Chebychev corrected were stitched. The algorithm and merge choice was Adjust XY Blend. This was chosen because as shown in Chapter 2 and in Hovis et al. that, excluding "overlay" there was minimal difference in the algorithm choice, so for this test the default was used [18]. After the stitches were complete, all three were filtered using a FFT band pass filter from 0.08 mm to 2.5 mm in accordance with ISO 10110 for the investigation of mid-spatial frequencies (waviness).

5.1.2 Results and Analysis

Figures 5-1 through 5-3 show the results of the stitches for the uncorrected, MATLAB corrected, and corrected by removing through 6th order Zernikes respectively. The W_q (waviness RMS according to ISO 10110) for all of the stitches are shown in Table 5-1.

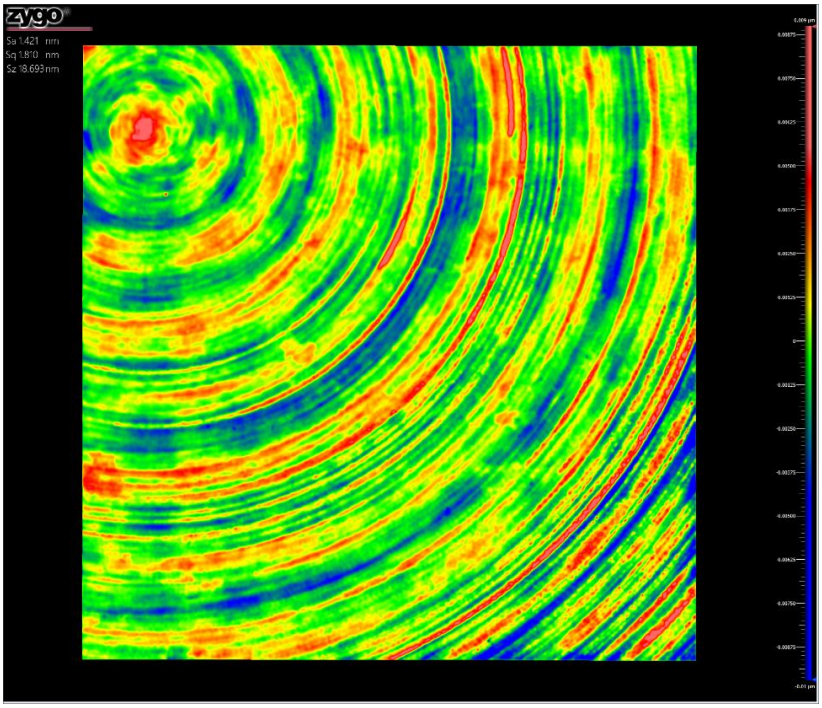

FIGURE 5-1: M1 with no correction.

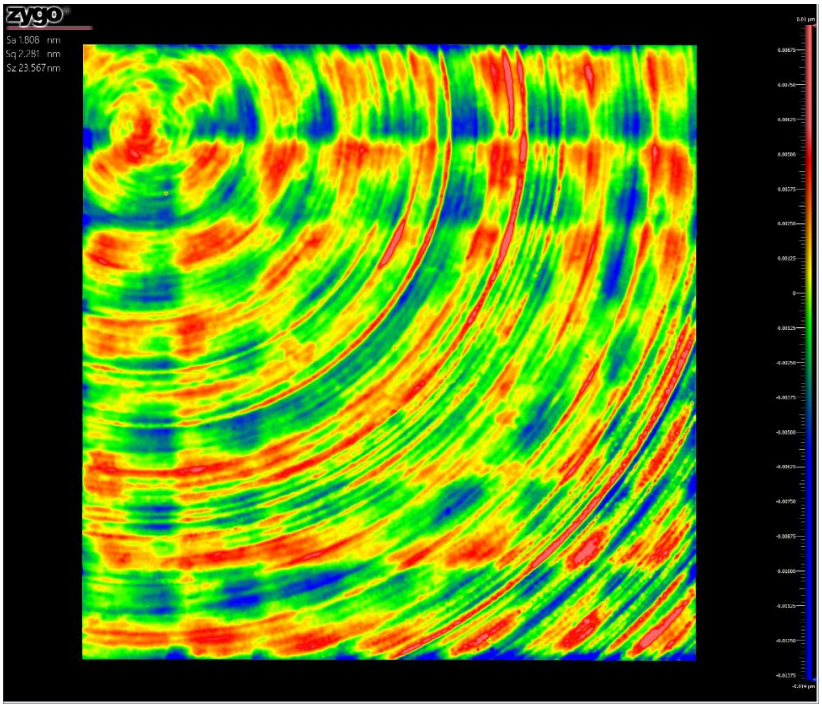

FIGURE 5-2: M1 with MATLAB correction.

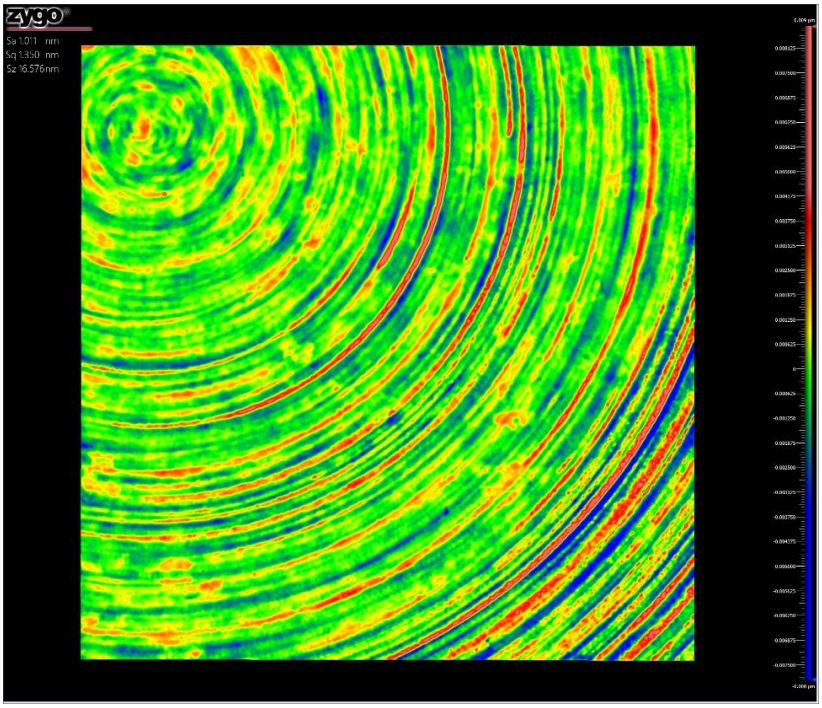

FIGURE 5-3: M1 with 6th Order Zernike removed from each site.

TABLE 5-1. W_q data for M1 stitching measurement.

Method	W_q (nm)
M1 Uncorrected	1.81
M1 MATLAB Correction	2.28
M1 6th Order Zernike Removal	1.35

The results in Figure 5-1 shows minor stitching artefacts, but also shows MSF at approximately 6 cycles over the approximately 17 mm x 17 mm FOV, or ~3 mm wavelength. Figure 5-2 showed the MATLAB correction made the W_q worse and appeared to create what looked like stitching artefacts. This is likely the result of uncertainty in the fit for the initial tip/tilt test. Important future work will be to relate quality of the fit (eg R^2) of the tip/tilt calibration data to the perceived quality of the correction where independent reference measurement exist. An earlier attempt at

correction, done with a different CSI and different test optics, had a higher data density calibration and led to more promising results.

For the 6th order Zernike removal correction, it was shown to reduce the W_q and looked closer to a traditional mid-spatial map. This does not mean these results are correct. With removing 6th order Zernikes, one could claim that they were only removing form from the measurement and not affecting the mid-spatial results; however, doing this could also easily affect the mid-spatial results. Neither result cannot be verified until future work is done and these results are compared to a different form of metrology.

5.2 Asphere Optic from NASA L'Ralph

This portion of the work was done at NASA Goddard Space Flight Center in conjunction with the L'Ralph project. This test was done to look specifically at the mid-spatials of the optic, not the figure or roughness. The optic under test was a diamond turned aluminum convex aspheric mirror, which was referred to as M2 for the L'Ralph project. Similar to 5.1 there was not a reference measurement for this optic. The correction methods outlined in 5.1 were applied.

5.2.1 Experimental Setup

To perform this optical test a Zygo NewView 8300 CSI with a 5.5x objective and a 0.5x tube lens (3 mm x 3 mm FOV) was used. Since the fringe density test was completed in 5.1.1, it was not repeated for this experiment. Stitching this optic was more complex and time consuming than the previous measurements, because the slopes of the asphere fell outside of the slope limit of the objective. To try and get some understanding of the mid-spatials multiple stitches were taken where the optic was tipped/tilted in

between the stitches, so each stitch fell inside the slope limit of the objective. The first stitch was a 3x3 stitch at the center of the optic. After the center stitch four 3x5 stitches were completed, with one going out in each direction from the center stitch. Next two more stitches were completed. Each was a 3x9 stitch coming from the 3x5 stitches on the long sides of the optic. This stitching set up resulted in cross pattern on the optic with the center of the optic at the center of the cross. This pattern on the optic can be seen in Figure 5-4.

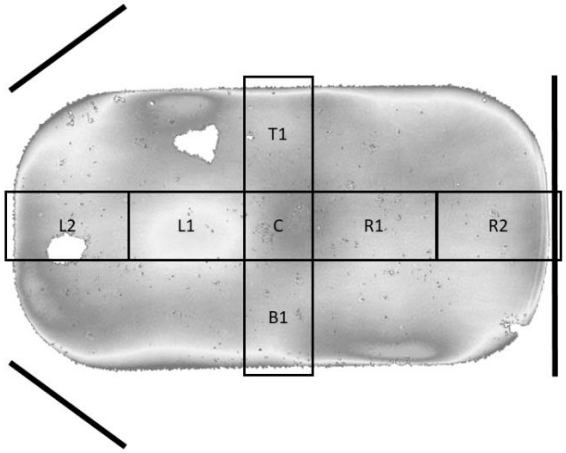

FIGURE 5-4: Map of the stitches that were measured (the lines on the outside help define the orientation of the optic)

5.2.2 Results and Analysis

Figure 5-5 through Figure 5-10, show the C (center) and B1 stitches of M2 (L'Ralph) for uncorrected, corrected with MATLAB, and corrected by removing through 6^{th} order Zernikes. The W_q (waviness RMS according to ISO 10110) for all of the stitches are shown in Table 5-2.

The stitched data for the center shows a FOV of approximately 7.8 mm square. The uncorrected data suggest a 50 nm amplitude MSF with a spatial wavelength of order 2.5 mm; the “corrected” data suggests a higher spatial frequency component; more data is required to improve the evaluation of MSF components. Note that stitching the 6th order Zernike removed surfaces suggests a high frequency radial “spoke” pattern at a higher frequency than would be expected from a motor pole pass frequency.

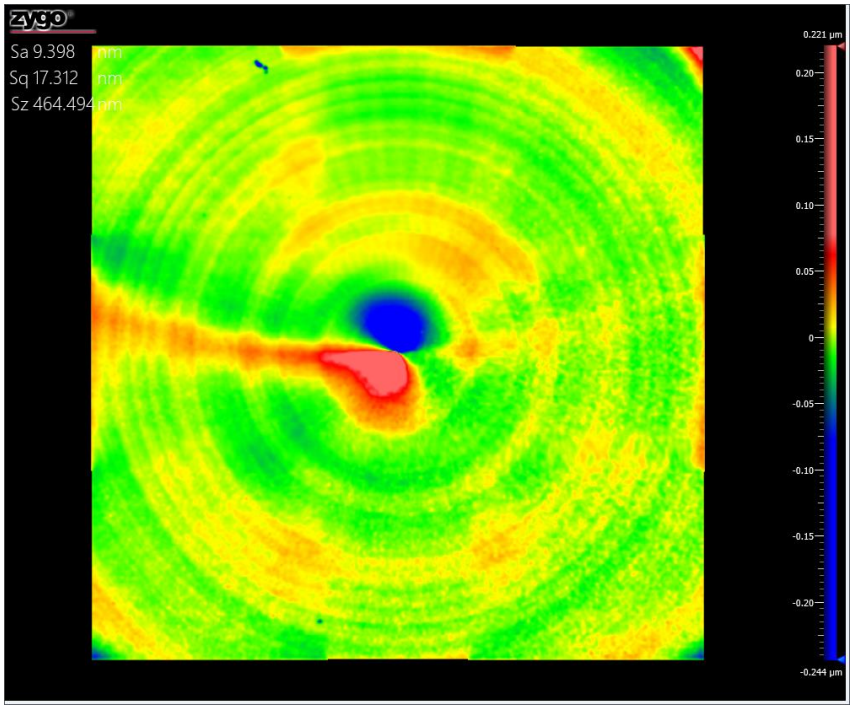

FIGURE 5-5: Center with no correction.

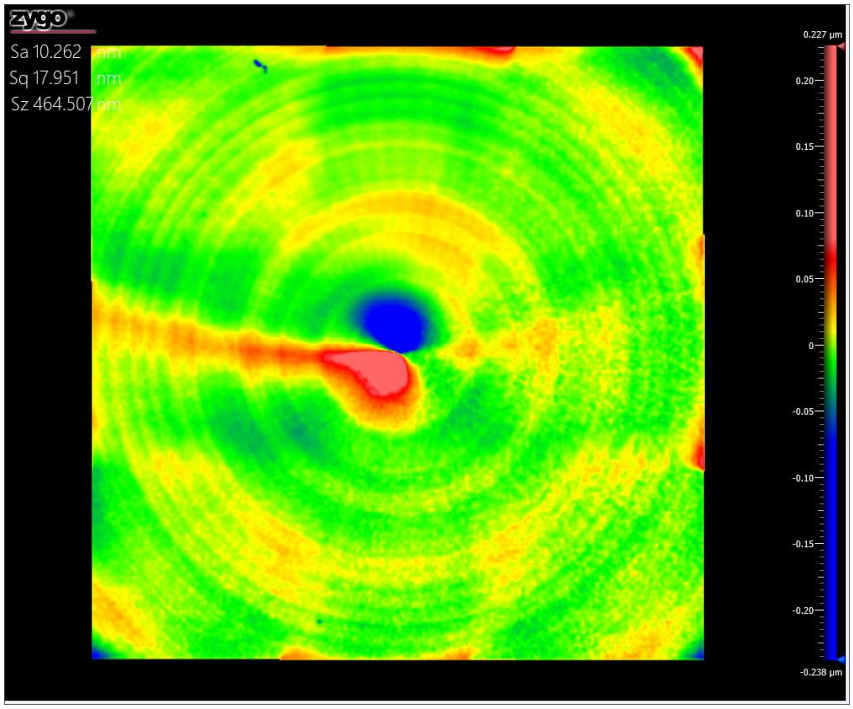

FIGURE 5-6: Center with MATLAB correction.

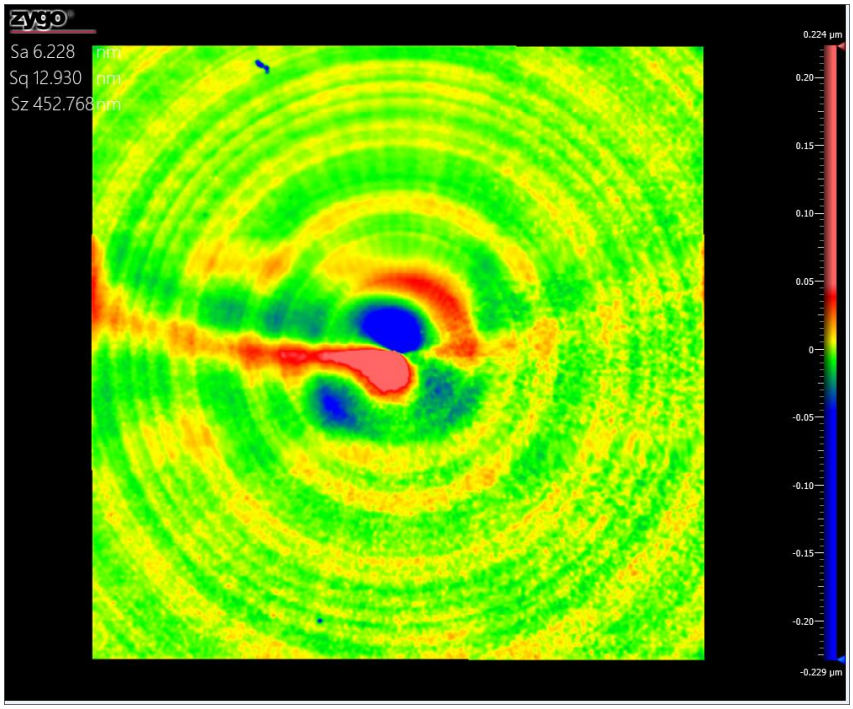

FIGURE 5-7: Center with 6th Order Zernike removed from each site.

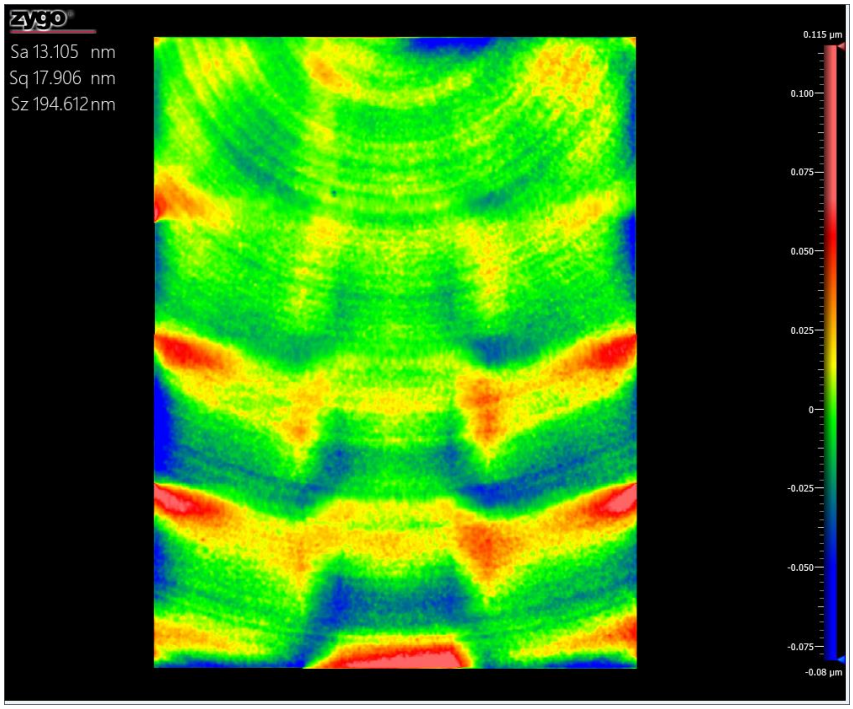

FIGURE 5-8: B1 with no correction.

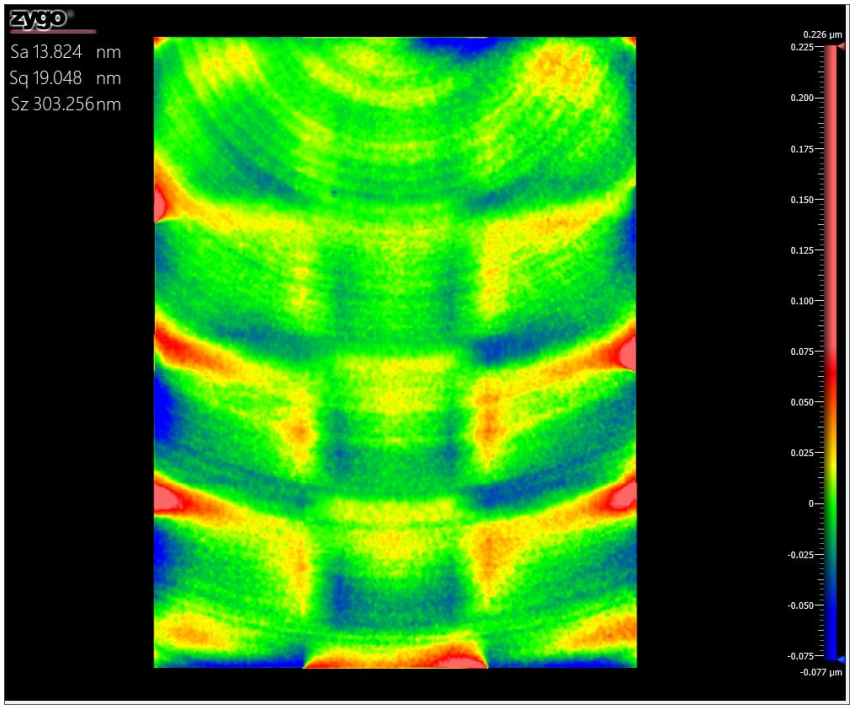

FIGURE 5-9: B1 with MATLAB correction

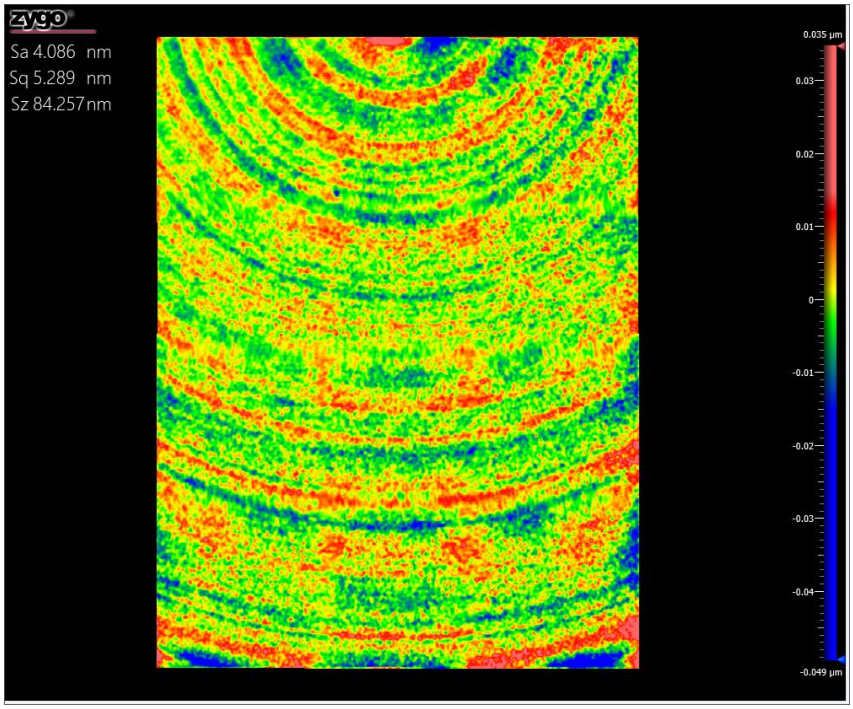

FIGURE 5-10: B1 with 6th Order Zernike removed from each site.

TABLE 5-2. W_q data for all M2 stitching measurements.

Site and Method	W_q (nm)
B1 Uncorrected	17.91
B1 6th Order Zernike Removal	5.29
B1 MATLAB Correction	19.05
Center Uncorrected	17.31
Center 6th Order Zernike Removal	12.93
Center MATLAB Correction	17.95
L1 Uncorrected	14.65
L1 6th Order Zernike Removal	5.51
L1 MATLAB Correction	16.91
L2 Uncorrected	29.80
L2 6th Order Zernike Removal	5.76

Site and Method	W_q (nm)
L2 MATLAB Correction	35.55
R1 Uncorrected	15.44
R1 6th Order Zernike Removal	5.59
R1 MATLAB Correction	19.76
R2 Uncorrected	37.94
R2 6th Order Zernike Removal	7.62
R2 MATLAB Correction	38.81
T1 Uncorrected	9.57
T1 6th Order Zernike Removal	4.44
T1 MATLAB Correction	12.68

The results for the uncorrected stitches showed very obvious retrace errors and stitching artefacts. The MATLAB correction visually appeared to have reduced these errors and artefacts, however, the W_q value actually went up. Similar to the results in 5.1.2 the initial fringe density test done is too sparse to make a proper correlation. Examples of this issue are shown in Figure 5-11 and Figure 5-12. The fit of the Chebyshev data in Chapter 3 was linear with few outliers. For this data, almost all of the fits were non-linear with many outliers, which makes it hard or impossible to interpolate the induced aberrations throughout the slope limit of the objective. Figure 5-12 shows that the fit for the Chebyshev power term is non-linear. This non-linearity can lead to the data either being under or over corrected, and it was shown in Chapter 4 that this type of aberration amplifies and propagates throughout the stitch. Future work for this project should include acquiring a higher density tip/tilt test to make a proper correlation between the fringe density and the retrace error for this CSI and objective.

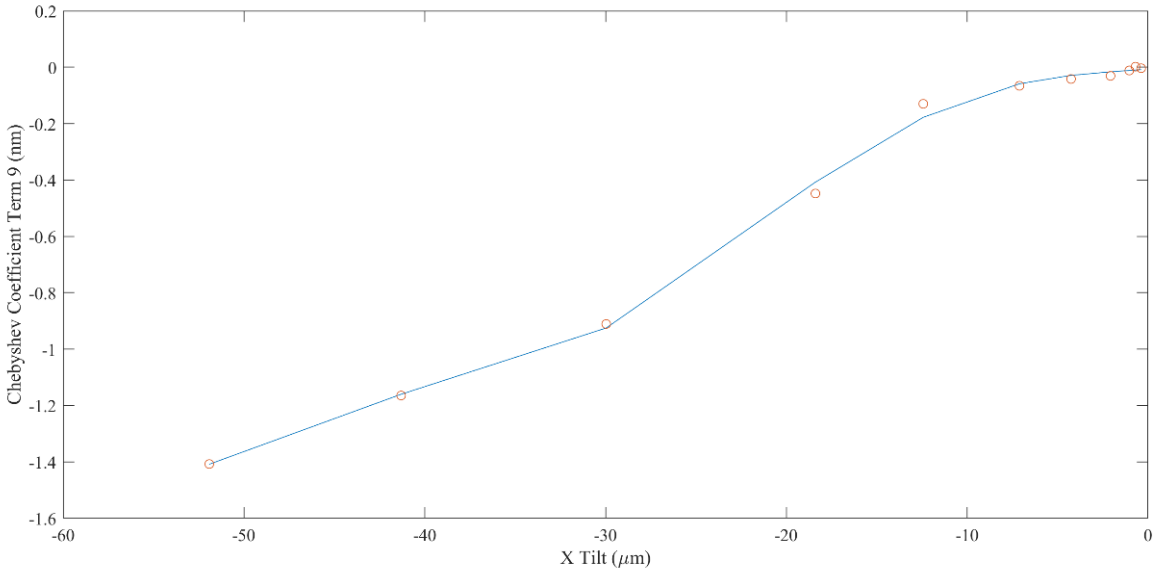

FIGURE 5-11: The data and fit for the Chebyshev X coma coefficient vs X tilt

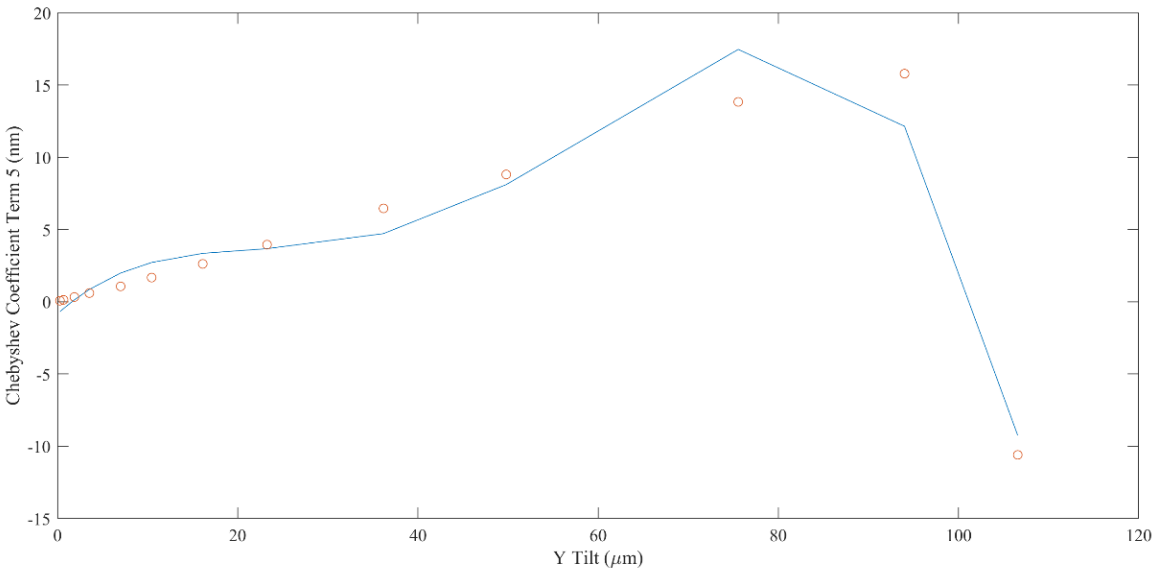

FIGURE 5-12: The data and fit for the Chebyshev power coefficient vs Y tilt

For the 6th order Zernike removal correction, it was shown to reduce the W_q by more than half except for the center stitch, and looked closer to a traditional mid-spatial map. Due to the way this Zernike removal was done, there were still the issues and questions talked about in 5.1.2.

These results reinforce earlier observations about the Zernike correction method and the importance of low uncertainty in the fits on which the Chebyshev based corrections are made.

CHAPTER 6: CONCLUSIONS AND FUTURE WORK

6.1 Conclusions

Using a CSI and utilizing stitching has the potential to measure form and mid-spatials on optics where it was previously too hard, too costly, or impossible to perform. Chapter 2 showed that a CSI and stitching can measure large areas on traditional and non-traditional optics. It was also shown that for a planar optic the results are comparable to traditional methods. The process, however, creates retrace errors when the measurement is acquired at a non-null fringe. Chapter 3 explored these retrace errors and the aberrations they create, which are orders of magnitude larger than the retrace errors themselves, when subjected to the stitching process. A correction of these errors was implemented. The results of the correction showed a promising change in the stitching results, removing a mid-spatial ripple in the stitch and reducing the $S_q\Delta$. This correction, however, did not mitigate all of the aberrations induced in the measurement. Chapter 4 looked into the possibility of an error in the reference propagating through the measurement. It was shown that a small 2 nm power error in the reference can rapidly become a 10 nm and 40 nm error in a 2x3 and 2x5 stitch respectively. The retrace correction was then expanded to a different CSI as well as different freeform and aspheric optics. Results showed issues with this expansion, which was found to be in the experimental data for the correlation between fringe density and induced errors. The data was too sparse to make an accurate correlation, which caused artefacts to be induced in the stitch.

6.2 Future Work

Future work for this project includes making the correction in MATLAB more robust, so it can be expanded to other instruments and optics easily. Another suggestion is to perform experimental tests to calculate the correlation between fringe density and retrace errors for higher magnification objectives with higher slope limits. Presumably, these will have larger retrace errors when measuring optics with these higher slopes. The final suggestion for future work is to also look more into the errors which are caused by the reference optics, either by using experimental and simulation data, or by performing a calibration procedure prior to any stitch.

REFERENCES

[1] Zygo Corporation, “Nexview Specifications SS-0098,” Retrieved from https://www.zygo.com/?sup=resource/manuals.cgi , (2013).

[2] J. Thunen and O. Kwon, “Full aperture testing with subaperture test optics,” Wavefront sensing; Proceedings of the Conference, San Diego, CA, August 1982.

[3] P. Murphy, G. Forbes, J. Fleig, P. Dumas, and M. Tricard, "Stitching interferometry: a flexible solution for surface metrology," Optics and Photonics News 14, 38-43 (2003).

[4] W. Chow and G. Lawrence, “Method for subaperture testing interferogram reduction”, Optics Letters, 8, 468-470, 1983.

[5] Gomez, Carlos, et al. "Optimization of surface measurement for metal additive manufacturing using coherence scanning interferometry." Optical Engineering 56.11 (2017): 111714.

[6] Jiang, Xiang. "Precision surface measurement." Phil. Trans. R. Soc. A370.1973 (2012): 4089-4114.

[7] Dutterer, Brian S., et al. "Diamond milling of an Alvarez lens in germanium." Precision Engineering 38.2 (2014): 398-408.

[8] Y. E. Tohme and J. A. Lowe, "Machining of Freeform Optical Surfaces by Slow Slide Servo Method," in Proceedings of the ASPE 2003 Annual Meeting.

[9] F. Fang, X. Zhang, A. Weckenmann, G. Zhang, and C. Evans, "Manufacturing and measurement of freeform optics," CIRP Annals-Manufacturing Technology 62, 823-846 (2013).

[10] C. Supranowitz, C. Maloney, P. Murphy, and P. Dumas, "Enhanced resolution and accuracy of freeform metrology through Subaperture Stitching Interferometry," in Optifab 2017, (International Society for Optics and Photonics, 2017), 1044818.

[11] Evans, C. and J. Bryan, “Compensation for errors introduced by nonzero fringe densities in phase-measuring interferometers,” CIRP Annals-Manufacturing Technology, 1993. 42(1): p. 577-580.

[12] Huang, C., “Propagation errors in precision Fizeau interferometry,” Applied optics, 1993. 32(34): p. 7016-7021.

[13] L. Deck and C. Evans, “High performance Fizeau and scanning white-light interferometers for mid-spatial frequency optical testing of free-form optics,” Proc. SPIE, 5921, 73–80 (2005).

[14] H. Kurita, K. Saito, M. Kato, and T. Yatagai, "Influeace of system aberrations on interferometric aspheric surface testing," in Surface Characterization and Testing, (International Society for Optics and Photonics, 1987), 47-54.

[15] J. E. Greivenkamp and A. E. Lowman, "Interferometer errors due to the presence of fringes," Applied optics 35, 6826-6828 (1996).

[16] Leslie L. Deck, "High precision interferometer for measuring mid-spatial frequency departure in free form optics," Proc. SPIE 10316, Optifab 2007: Technical Digest, 103160N (14 May 2007).

[17] C. Evans, “Compensation for errors introduced by non-zero fringe densities in phase-measuring interferometers,” CIRP Annals, 42/1, 577–580 (1993).

[18] Hovis, C., Reese, Z., Shahinian, H., and Evans, C., “Observations on Stitching Interferometry on Parts with Radically Different Surface Topographies,” In ASPE 32nd annual meeting, Charlotte, NC, USA. 2017.

[19] Zygo Corperation, “Verifire Specifications SS-0115,” Retrieved from https://www.zygo.com/?/met/interferometers/verifire/ , (2017).

[20] Zygo Corporation, “Mx: Reference Guide OMP-0550.” Retrieved from https://www.zygo.com/?sup=resource/manuals.cgi , (2015).

[21] QED Technologies, “Q-22XE Reference Guide MAN1234-D,” (2012).

[22] Michael U. Uwakwe and Christopher J. Evans. "Minimizing Task-Specific Uncertainty in CMM-Based Freeform Optics Metrology,” (2017).

[23] ISO/FDIS, “25178-2 2010 Areal - Terms, definitions and surface texture parameters,” (2010).

APPENDIX: MATLAB CODE

Reader.m:

```
clear all;
close all;
clc;
addpath(genpath('/users/chovis6/Freeform1/Sub1'));

fs = 30;%fontsize on plots
pd =40;%part diameter in mm
dd = 35;%desired diameter after cropping
nn = 150;%
ds = 802;%desired size in pixels
sc = 10^9;%height data scaler
ft = 'poly11';%form removal from data
ftn = 'linearinterp';%2d interpolation
Ydir='normal';%direction of the plots
MRRA='n';%material removal assessment? (for spot tests) y yes n no
nmask=1;%number of needed masks
filtering='FFT';%filtering needed> y yes n no
Lc=200;%low pass cutoff wavelength (mm)
Hc=0.2;%high pass cutoff wavelength (mm)
pnl=1;%process number indicator in the same location
fex='dat';%file extension
v = [0 90];%view of the mesh
Yl = 'height (nm)';%ylabel general profiles
Xl = 'Position (mm)';%xaxis label
Yli = 'Position (mm)';%xlabel (interferograms
Xli = 'Position (mm)';%axis label
Zl = 'Height (nm)';%legend label
Xlp = 'Frequency (1/mm)';%xlabel psd
Ylp = 'PSD (\mum^3)';%ylabel psd
Ylr = 'Height (nm)';%ylabel radial average profiles
Xlr = 'Position (mm)';%xlabel radial average
cmp = 'jet';%color map type for interferogram
cb = 'b';%blue plot color
ABH=2000;%symmetric height limit on the axes
ABL=10*round(pd/20);%absolute length value
cmpr = [-ABH ABH];%color map range
axr = [0 ABL -ABH ABH];%radial average profile limits

axrr = [0 ABL -ABH ABH];%radial average profile limits
```

```
axrd=[-ABL ABL -ABH ABH];%full diameter plot
lw=4;
int='linear';%interpolation methods
cb = 'b';%blue plot color
% cmpr = [-100 100];%color map rangervars -except mt sn side

addd=pwd;
addpath(addd);
workingfolder=pwd;
cd(workingfolder);
structname=dir;
namestruct={structname.name}.';
for i=3:length(namestruct)
   nnf=strsplit(char(namestruct(i)),'.');
   if strcmp(nnf(length(nnf)),'dat')
      n = char(nnf(1));
      Fizeau_analyzer_res;
   end

end
save('adptadj_avg.mat')
```

Analyzer.m:

```
ext = strcat('.',fex);
eval (sprintf('fname = strcat(n,ext);'));
ffnum=strsplit(n,'_');
if isnumeric(pnl)==1
   fnum=char(ffnum(pnl));
   fnum=str2num(fnum(2));
   eval(sprintf('n_%d=n;',fnum));%storing names
end
eval(sprintf('PM_%s = ReadZygoBinary(fname)*sc;',n));%read the phasemap

eval(sprintf('ds0 = max(size(PM_%s));',n));%the dimension of the loaded file
if ds0<ds
   ds=ds0;
end

st=sprintf('PM_%s',n);

eval(sprintf('[C,D] = NAN_Help(PM_%s);',n,n));
eval(sprintf('PM_%s = NAN_Fill(PM_%s);',n,n));
```

```
eval(sprintf(' dx = pd/length(cropper(PM_%s,0));',n,n));%cropping data to interferorgram limits %changed from PM_%s_res
ep=(pd-dd)/dx/2;
eval(sprintf('PM_%s = cropper(PM_%s,ep);',n,n));%cropping data to interferorgram limits
eval(sprintf('[ny,nx]=size(PM_%s);',n));%
eval(sprintf('R=fix(length(PM_%s)/2);',n));%
eval(sprintf('PM_%s=masker3c(PM_%s,fix(nx/2),fix(ny/2),R);',n,n));%
eval(sprintf('PM_%s=cropper(PM_%s,0);',n,n));%material removal
eval(sprintf('nrs_%s = ds/max(size(PM_%s));',n,n));%the dimension of the loaded file

eval(sprintf('[x,y]=cart_coord_C(PM_%s,dx,dx);',n));%creating cartesian coordinates with origin at the center of the interferogram %changed from PM_%s_res
eval(sprintf('tilt_%s = Spatial_interp(x,y,PM_%s,ft);',n,n));%calcualtion of tilt %changed from PM_%s_res
eval(sprintf('IFG_%s = PM_%s - tilt_%s(x,y);',n,n,n));%titlt subtraction %changed from PM_%s_res
eval(sprintf('IFG_%s=NAN_I(IFG_%s,dx,dx);',n,n));%filling the data missing

if strcmp(filtering, 'gaussian')% filtering portion
   eval(sprintf('IFG_%s=gaussf3bp(IFG_%s,dx,dx,Lc,Hc);',n,n));%filling the data missing

elseif strcmp(filtering, 'FFT')
   eval(sprintf('IFG_%s=fftfilter3(IFG_%s,Lc,Hc,dx,dx);',n,n));%filling the data missing
end

eval(sprintf('[x,y]=cart_coord_C(IFG_%s,dx,dx);',n));%new cartesian coordinates for cropped data
eval(sprintf('[ny,nx]=size(IFG_%s);',n));

%eval(sprintf('r_%s = ravo(IFG_%s);',n,n));%radial average profile
%eval(sprintf('xr_%s = transpose((1:length(r_%s))*dx);',n,n));

eval(sprintf('IFG_%s_res=imresize(IFG_%s,nrs_%s);',n,n,n));

eval(sprintf('[x_res,y_res]=cart_coord_C(IFG_%s_res,dx,dx);',n));%new cartesian coordinates for cropped data
eval(sprintf('[ny_res,nx_res]=size(IFG_%s_res);',n));

%eval(sprintf('r_%s_res = ravo(IFG_%s_res);',n,n));%radial average profile
%eval(sprintf('xr_%s_res = transpose((1:length(r_%s_res))*dx);',n,n));

%% Parameter check
```

```
eval(sprintf('Sq_%s=rms2d(IFG_%s);',n,n));
eval(sprintf('Sq_%s_res=rms2d(IFG_%s_res);',n,n));
eval(sprintf('pv_%s_res=PeaktoValley(IFG_%s_res);',n,n));
eval(sprintf('pv_%s=PeaktoValley(IFG_%s);',n,n));
%% intergerogram map plot and radial average profiles


eval(sprintf('p_%s=only_im(IFG_%s,cmp,cmpr,n);',n,n));%3d contour graph of the
interferogram
rn = sprintf('res_%s',n);
eval(sprintf('p_%s_res=only_im(IFG_%s_res,cmp,cmpr,rn);',n,n));
```

Subtraction.m:

```
clear all;
close all;
clc;

addpath(genpath('/users/chovis6/SubtractFreeform/Sub2'));

load('xy_avg.mat')
xy_avg = IFG_Freeform_Xy_Avg;
xy_avg_res = IFG_Freeform_Xy_Avg_res;
clearvars -except Sq* xy*

load('xy_blend.mat')
xy_blend = IFG_Freeform_Xy_Blend;
xy_blend_res = IFG_Freeform_Xy_Blend_res;
clearvars -except Sq* xy*

load('xy_no.mat')
xy_no = IFG_Freeform_Xy_No;
xy_no_res = IFG_Freeform_Xy_No_res;
clearvars -except Sq* xy*

load('over_avg.mat')
over_avg = IFG_Freeform_Over_Avg;
over_avg_res = IFG_Freeform_Over_Avg_res;
clearvars -except Sq* xy* over*

load('over_blend.mat')
over_blend = IFG_Freeform_Over_Blend;
over_blend_res = IFG_Freeform_Over_Blend_res;
```

```
clearvars -except Sq* xy* over*

load('over_no.mat')
over_no = IFG_Freeform_Over_No;
over_no_res = IFG_Freeform_Over_No_res;
clearvars -except Sq* xy* over*

load('cart_avg.mat')
cart_avg = IFG_Freeform_Cart_Avg;
cart_avg_res = IFG_Freeform_Cart_Avg_res;
clearvars -except Sq* xy* over* cart*

load('cart_blend.mat')
cart_blend = IFG_Freeform_Cart_Blend;
cart_blend_res = IFG_Freeform_Cart_Blend_res;
clearvars -except Sq* xy* over* cart*

load('cart_no.mat')
cart_no = IFG_Freeform_Cart_No;
cart_no_res = IFG_Freeform_Cart_No_res;
clearvars -except Sq* xy* over* cart*

load('adptadj_avg.mat')
adptadj_avg = IFG_Freeform_AdptAdj_Avg;
adptadj_avg_res = IFG_Freeform_AdptAdj_Avg_res;
clearvars -except Sq* xy* over* cart* adptadj*

load('adptadj_blend.mat')
adptadj_blend = IFG_Freeform_AdptAdj_Blend;
adptadj_blend_res = IFG_Freeform_AdptAdj_Blend_res;
clearvars -except Sq* xy* over* cart* adptadj*

load('adptadj_no.mat')
adptadj_no = IFG_Freeform_AdptAdj_No;
adptadj_no_res = IFG_Freeform_AdptAdj_No_res;
clearvars -except Sq* xy* over* cart* adptadj*

load('Fiz.mat')
fiz = IFG_Freeform_Fiz;
clearvars -except Sq* xy* over* cart* adptadj* fiz*

adptadj_a_b = adptadj_avg - adptadj_blend;
adptadj_a_n = adptadj_avg - adptadj_no;
adptadj_b_n = adptadj_blend - adptadj_no;
```

```
Sq_adptadj_a_b=rms2d(adptadj_a_b);
Sq_adptadj_a_n=rms2d(adptadj_a_n);
Sq_adptadj_b_n=rms2d(adptadj_b_n);

adptadj_a_b_res = adptadj_avg_res - adptadj_blend_res;
adptadj_a_n_res = adptadj_avg_res - adptadj_no_res;
adptadj_b_n_res = adptadj_blend_res - adptadj_no_res;
Sq_adptadj_a_b_res = rms2d(adptadj_a_b_res);
Sq_adptadj_a_n_res = rms2d(adptadj_a_n_res);
Sq_adptadj_b_n_res = rms2d(adptadj_b_n_res);

cart_a_b = cart_avg - cart_blend;
cart_a_n = cart_avg - cart_no;
cart_b_n = cart_blend - cart_no;
Sq_cart_a_b=rms2d(cart_a_b);
Sq_cart_a_n=rms2d(cart_a_n);
Sq_cart_b_n=rms2d(cart_b_n);

cart_a_b_res = cart_avg_res - cart_blend_res;
cart_a_n_res = cart_avg_res - cart_no_res;
cart_b_n_res = cart_blend_res - cart_no_res;
Sq_cart_a_b_res=rms2d(cart_a_b_res);
Sq_cart_a_n_res=rms2d(cart_a_n_res);
Sq_cart_b_n_res=rms2d(cart_b_n_res);

over_a_b = over_avg - over_blend;
over_a_n = over_avg - over_no;
over_b_n = over_blend - over_no;
Sq_over_a_b=rms2d(over_a_b);
Sq_over_a_n=rms2d(over_a_n);
Sq_over_b_n=rms2d(over_b_n);

over_a_b_res = over_avg_res - over_blend_res;
over_a_n_res = over_avg_res - over_no_res;
over_b_n_res = over_blend_res - over_no_res;
Sq_over_a_b_res=rms2d(over_a_b_res);
Sq_over_a_n_res=rms2d(over_a_n_res);
Sq_over_b_n_res=rms2d(over_b_n_res);

xy_a_b = xy_avg - xy_blend;
xy_a_n = xy_avg - xy_no;
xy_b_n = xy_blend - xy_no;
Sq_xy_a_b=rms2d(xy_a_b);
Sq_xy_a_n=rms2d(xy_a_n);
```

```
Sq_xy_b_n=rms2d(xy_b_n);

xy_a_b_res = xy_avg_res - xy_blend_res;
xy_a_n_res = xy_avg_res - xy_no_res;
xy_b_n_res = xy_blend_res - xy_no_res;
Sq_xy_a_b_res=rms2d(xy_a_b_res);
Sq_xy_a_n_res=rms2d(xy_a_n_res);
Sq_xy_b_n_res=rms2d(xy_b_n_res);

a_xy_cart_res = xy_avg_res - cart_avg_res;
b_xy_cart_res = xy_blend_res - cart_blend_res;
n_xy_cart_res = xy_no_res - cart_no_res;
Sq_a_xy_cart_res=rms2d(a_xy_cart_res);
Sq_b_xy_cart_res=rms2d(b_xy_cart_res);
Sq_n_xy_cart_res=rms2d(n_xy_cart_res);

a_xy_over_res = xy_avg_res - over_avg_res;
b_xy_over_res = xy_blend_res - over_blend_res;
n_xy_over_res = xy_no_res - over_no_res;
Sq_a_xy_over_res=rms2d(a_xy_over_res);
Sq_b_xy_over_res=rms2d(b_xy_over_res);
Sq_n_xy_over_res=rms2d(n_xy_over_res);

a_xy_adptadj_res = xy_avg_res - adptadj_avg_res;
b_xy_adptadj_res = xy_blend_res - adptadj_blend_res;
n_xy_adptadj_res = xy_no_res - adptadj_no_res;
Sq_a_xy_adptadj_res=rms2d(a_xy_adptadj_res);
Sq_b_xy_adptadj_res=rms2d(b_xy_adptadj_res);
Sq_n_xy_adptadj_res=rms2d(n_xy_adptadj_res);

a_cart_over_res = cart_avg_res - over_avg_res;
b_cart_over_res = cart_blend_res - over_blend_res;
n_cart_over_res = cart_no_res - over_no_res;
Sq_a_cart_over_res=rms2d(a_cart_over_res);
Sq_b_cart_over_res=rms2d(b_cart_over_res);
Sq_n_cart_over_res=rms2d(n_cart_over_res);

a_cart_adptadj_res = cart_avg_res - adptadj_avg_res;
b_cart_adptadj_res = cart_blend_res - adptadj_blend_res;
n_cart_adptadj_res = cart_no_res - adptadj_no_res;
Sq_a_cart_adptadj_res=rms2d(a_cart_adptadj_res);
Sq_b_cart_adptadj_res=rms2d(b_cart_adptadj_res);
Sq_n_cart_adptadj_res=rms2d(n_cart_adptadj_res);
```

```
a_over_adptadj_res = over_avg_res - adptadj_avg_res;
b_over_adptadj_res = over_blend_res - adptadj_blend_res;
n_over_adptadj_res = over_no_res - adptadj_no_res;
Sq_a_over_adptadj_res=rms2d(a_over_adptadj_res);
Sq_b_over_adptadj_res=rms2d(b_over_adptadj_res);
Sq_n_over_adptadj_res=rms2d(n_over_adptadj_res);


fs = 30;%fontsize on plots
pd =40;%part diameter in mm
dd = 35;%desired diameter after cropping
nn = 150;%
ds = 802;%desired size in pixels
sc = 10^9;%height data scaler
ft = 'poly11';%form removal from data
ftn = 'linearinterp';%2d interpolation
Ydir='normal';%direction of the plots
v = [0 90];%view of the mesh
Yl = 'height (nm)';%ylabel general profiles
Xl = 'Position (mm)';%xaxis label
Yli = 'Position (mm)';%xlabel (interferograms
Xli = 'Position (mm)';%axis label
Zl = 'Height (nm)';%legend label
Xlp = 'Frequency (1/mm)';%xlabel psd
Ylp = 'PSD (\mum^3)';%ylabel psd
Ylr = 'Height (nm)';%ylabel radial average profiles
Xlr = 'Position (mm)';%xlabel radial average
cmp = 'jet';%color map type for interferogram
cb = 'b';%blue plot color
ABH=2000;%symmetric height limit on the axes
ABL=10*round(pd/20);%absolute length value
cmpr = [-ABH ABH];%color map range

subtracter1;
subtracter2;
subtracter3;
subtracter4;
subtracter5;
subtracter6;
subtracter7;
subtracter8;
subtracter9;
subtracter10;
subtracter11;
```

subtracter12;

```
addpath(genpath('/users/chovis6/SubtractFreeform/SubZern'));
dx=dd/ds;
[RMSRI_AA, RSMRV_AA, ZRIt_AA, ZRVt_AA] = ZernCalc(adptadj_avg_res,dx);
[RMSRI_AB, RSMRV_AB, ZRIt_AB, ZRVt_AB] = ZernCalc(adptadj_blend_res,dx);
[RMSRI_AN, RSMRV_AN, ZRIt_AN, ZRVt_AN] = ZernCalc(adptadj_no_res,dx);
[RMSRI_CA, RSMRV_CA, ZRIt_CA, ZRVt_CA] = ZernCalc(cart_avg_res,dx);
[RMSRI_CB, RSMRV_CB, ZRIt_CB, ZRVt_CB] = ZernCalc(cart_blend_res,dx);
[RMSRI_CN, RSMRV_CN, ZRIt_CN, ZRVt_CN] = ZernCalc(cart_no_res,dx);
[RMSRI_OA, RSMRV_OA, ZRIt_OA, ZRVt_OA] = ZernCalc(over_avg_res,dx);
[RMSRI_OB, RSMRV_OB, ZRIt_OB, ZRVt_OB] = ZernCalc(over_blend_res,dx);
[RMSRI_ON, RSMRV_ON, ZRIt_ON, ZRVt_ON] = ZernCalc(over_no_res,dx);
[RMSRI_XA, RSMRV_XA, ZRIt_XA, ZRVt_XA] = ZernCalc(xy_avg_res,dx);
[RMSRI_XB, RSMRV_XB, ZRIt_XB, ZRVt_XB] = ZernCalc(xy_blend_res,dx);
[RMSRI_XN, RSMRV_XN, ZRIt_XN, ZRVt_XN] = ZernCalc(xy_no_res,dx);
[RMSRI_Fiz, RSMRV_Fiz, ZRIt_Fiz, ZRVt_Fiz] = ZernCalc(fiz,dx);

rmpath('/users/chovis6/SubtractFreeform/Sub2');
addpath(genpath('/users/chovis6/SubtractFreeform/SubPsd'));
dx=dd/ds;
[Freq_AA, Psd_AA] = psdrun(adptadj_avg_res,dd,dx);
[Freq_AB, Psd_AB] = psdrun(adptadj_blend_res,dd,dx);
[Freq_AN, Psd_AN] = psdrun(adptadj_no_res,dd,dx);
[Freq_CA, Psd_CA] = psdrun(cart_avg_res,dd,dx);
[Freq_CB, Psd_CB] = psdrun(cart_blend_res,dd,dx);
[Freq_CN, Psd_CN] = psdrun(cart_no_res,dd,dx);
[Freq_OA, Psd_OA] = psdrun(over_avg_res,dd,dx);
[Freq_OB, Psd_OB] = psdrun(over_blend_res,dd,dx);
[Freq_ON, Psd_ON] = psdrun(over_no_res,dd,dx);
[Freq_XA, Psd_XA] = psdrun(xy_avg_res,dd,dx);
[Freq_XB, Psd_XB] = psdrun(xy_blend_res,dd,dx);
[Freq_XN, Psd_XN] = psdrun(xy_no_res,dd,dx);
[Freq_Fiz, Psd_Fiz] = psdrun(fiz,dd,dx);

save('subtractFree.mat')
```

subtracter1.m:

```
%% subtracting to specific measurements
iter=3;
Zerncalc=0;%do you want zernikie calculation(1 yes 0 no);
pmask=100;%percentage data masked for subtraction
```

```
fs=30;
ms=802;%size measurements will be fitted
nrms=50000;%number for spike clipping above n times of the surface rms
dd = 35;
dx_new=dd/ms;
dx=dx_new;
Rmp=pmask*ms/200;
m='linear';
na = sprintf('xy_avg_res');
nb = sprintf('fiz');
eval(sprintf('IFG_%s=aspect_r(%s,ms,1);',na,na));
eval(sprintf('IFG_%s=aspect_r(%s,ms,1);',nb,nb));
ZTO=6;
dt=0.5;%angle rotation increment for alignment of measurement
sfx =sprintf('_pFizXyA');



eval(sprintf('[Sub_%s theta_%s] =
subtract(IFG_%s,IFG_%s,1,ms,20,5,m);',sfx,sfx,na,nb));%calucaltion of the
subtractioneval(sprintf('dx_new = dd/length(Sub_%s);',sfx));%new spacing due to matrix
resize
eval(sprintf('Sub_spc_%s = spclip(Sub_%s,m,nrms);',sfx,sfx));%clipping spikes of the
subtraction map
eval(sprintf('Sub_spcm_%s = masker3c(Sub_%s,fix(ms/2),fix(ms/2),Rmp);',sfx,sfx));
eval(sprintf('Sub_spc_%s = Sub_spc_%s-
mean(mean(NAN_OR(Sub_spc_%s,dx,dx)));',sfx,sfx,sfx));%clipping spikes of the
subtraction map
eval(sprintf('MRcsub_spc_%s=sum(sum(NAN_R(Sub_spc_%s)))/10^-
3*dx^2*10^6;',sfx,sfx));
%{
eval(sprintf('rsub_%s = ravo(cropper(Sub_spc_%s,0));',sfx,sfx));%radial average profile
eval(sprintf('xrsub_%s = transpose((1:length(rsub_%s))*dx);',sfx,sfx));
%}
%% plotting the subtraction

eval(sprintf('[x_sub,y_sub]=cart_coord_C(Sub_spc_%s,dx_new,dx_new);',sfx));%new
cartesian coordinates for cropped data
Yli = 'Position (mm)';%xlabel
Zl = 'Height (nm)';%legend label
% axr = [min(min(x_sub)) max(max(x_sub)) min(min(y_sub)) max(max(y_sub))];% axis
range
v = [0 90];%view of the mesh
```

```
eval(sprintf('RMS_sub_%s= num2str(rms2d(Sub_spc_%s))',sfx,sfx));%rms of the
subtraction map
%Xli = sprintf('RMS is %s nm',RMS_sub);%printing the rms error of the interferogram
on the xaxis
eval(sprintf('p_sub_%s=only_im(Sub_spc_%s,cmp,cmpr,sfx);',sfx,sfx));%3d contour
graph of the interferogram

Ylr = 'Height (nm)';%xlabel
Xlr = 'Position (mm)';%xlabel
nr = sprintf ('rsubave_%s',sfx);%name of file plot to be saved to


%% zernike caculation and graphs
if Zerncalc==1
    eval(sprintf('Mask=zeros(size(Sub_spc_%s));',sfx));
    eval(sprintf('kmm=find(isnan(Sub_spc_%s)==1);',sfx));
    Mask(kmm)=nan;
    eval(sprintf('[x_sub,y_sub]=cart_coord_C(Sub_spc_%s,dx_new,dx_new);',sfx));%new
cartesian coordinates for cropped data
    Zernike_calculator
    eval(sprintf('ZRI_%s=
spatial_fit_3d_custom(x_sub,v1,y_sub,v2,Sub_%s,char(Ztri));',sfx,sfx));%calculation of
RI terms
    eval(sprintf('ZRV_%s=
spatial_fit_3d_custom(x_sub,v1,y_sub,v2,Sub_%s,char(Ztrv));',sfx,sfx));%calculation of
RV terms
    eval(sprintf('ZRIm_%s= ZRI_%s(x_sub,y_sub)+Mask;',sfx,sfx));%calculation of RI
terms
    eval(sprintf('rrisub_%s = ravo(ZRI_%s(x_sub,y_sub));',sfx,sfx));%radial average
profile
    eval(sprintf('Drisub_%s=[fliplr(rrisub_%s) rrisub_%s];',sfx,sfx,sfx));%creating the full
profile
    eval(sprintf('xrrisub_%s = transpose((1:length(rrisub_%s))*dx);',sfx,sfx));
    eval(sprintf('rrisubp_%s=fullplot(xrrisub_%s,Xlr,rrisub_%s-
mean(rrisub_%s),Ylr,Ydir,3,fs,axrr,cb,nr);',sfx,sfx,sfx,sfx));%plot

    eval(sprintf('ZRVm_%s= ZRV_%s(x_sub,y_sub)+Mask;',sfx,sfx));%calculation of RV
terms
    %RI terms
    sfxri=strcat(sfx,'RI');
    eval(sprintf('RMS_ZRI= num2str(rms2d(ZRIm_%s))',sfx));%rms of the subtraction
map
    Xli = sprintf('RMS is %s nm',RMS_ZRI);%printing the rms error of the interferogram
on the xaxis
```

```
    eval(sprintf('p_ZRI_%s=only_im(ZRIm_%s,cmp,cmpr,sfxri);',sfx,sfx));%3d contour
graph of the interferogram

    %RV terms
    sfxrv=strcat(sfx,'RV');
    eval(sprintf('RMS_ZRV= num2str(rms2d(ZRVm_%s))',sfx));%rms of the subtraction
map
    Xli = sprintf('RMS is %s nm',RMS_ZRV);%printing the rms error of the interferogram
on the xaxis
    eval(sprintf('p_ZRV_%s=only_im(ZRVm_%s,cmp,cmpr,sfxrv);',sfx,sfx));%3d contour
graph of the interferogram
end
```